POLITECNICO DI TORINO

Corso di Laurea in Ingegneria Aerospaziale

Tesi di Laurea Magistrale

MDO analysis of composite wing

Relatore
Prof. Erasmo Carrera

Correlatore:
Dr. Alfonso Pagani

Maria Pia Lionetti
matricola: 241427

Anno accademico 2018 – 2019

Contents

Chapter 1

Introduction

Sometimes the level of structural complexity exceeds our ability to make design changes, especially in aerospace engineering, where a single design is performed by different teams, each one focusing on a different subject. It goes without saying that the final target of the different teams is the same, for example minimizing the structural weight.
Multidisciplinary design optimization (MDO) is exactly the field of engineering that uses optimization methods to solve design problems incorporating a number of disciplines. Design optimization is the process of generating improved design through the use of different algorithms. This process is performed by an optimizer, which, in order to achieve the best solution, uses the design sensitivity coefficients. The latter describe the rates of change of structural responses with respect to changes in design parameters. They usually represent beam cross section dimensions, shell thicknesses and so on.
When performing optimization design, we must set a goal to achieve. Suppose we want to find the point of lowest elevation of an hill: this is called the "objective". Suppose that we want to study only a portion of the hill: we are setting some "constraints" that act as bounds in our "design space", which is the region the defines all of our possible position on the hill.
There are different algorithms available that we can use when searching for an optimum. NX Nastran, for example, uses a gradient-based algorithm. This kind of algorithm determine the direction in which to search using the gradients of the objective function and constraints. Moreover, there are several issues to be highlighted. First of all it should be underlined that not every optimization analysis leads to a feasible solution. Say we want to change a plate's thickness in order to limit the deformation under load. If we impose overly stringent constraints to the variation of the thickness, we could not find the solution sought.
Furthermore, the solution to an optimization problem is not singular. It means that, if we change the initial conditions or the algorithm used, we may obtain a different solution. This is particularly noticeable when using a gradient-based algorithm, since, it inherently looks for a local minimum and not for a global one. So, if we want to find the minimum of an irregolar function, we will have different solution depending on the starting point chosen.

Chapter 2

Composites materials

Composites materials are used in a wide variety of market, including structures, energy, automotive and aerospace. In particular, in the aerospace industry, where saving weight and increasing safety is a highly significant topic, the use of composites materials allowed to improve structures, dealing with always new challenges such as environmental regulations and fuel cost increasing.
As early as in the 1950s, fiberglass was used in the design of the Boeing 707 passenger jet and, in the 1960s, Rolls Royce introduced carbon fiber in the design of the compressor blades of the RB211 jet engine. In the first stage of the development of composites, they were used only in small amount in military aircraft and they became available in civil aviation since the 1960s.
In a short time composites have primarily been used for secondary wing and tail components such as wing trailing edge panels and rudders. Nowadays, modern aircraft are commonly made up of 50% to 70% composite material, since this provides benefits over different issues, such as:

- weight reduction up to 50%;
- higher impact resistance;
- higher resistance to fatigue and corrosion;
- easy to assemble.

Composite materials are made from two or more materials, called *constituent*, with different physical or chemical properties that, once combined, produce a material with different characteristics from the individual components, depending on the way the constituent are put together.
Depending on the constituent and on the way they are combined, composite materials can be classified in different ways. First of all, constituent can be organic (wood, for instance) or inorganic (metals). Organic composites are often avoided when high stiffness and strength are needed, furthermore, this kind of composite is too sensitive to environmental effects such as moisture. A different classification relies on the nature of the constituent is derived. For instance, we can identify four different classes of composites: particulate composite,

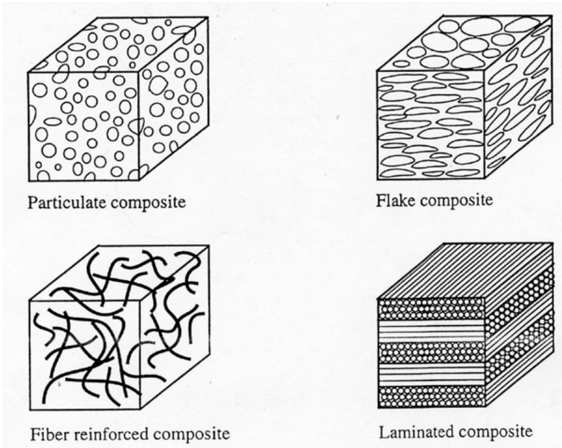

Figure 2.1

flake composite, fiber reinforced composite and laminate composite.

The following dissertation will be focused on the use of laminate composite, which is a material made of thin layers fully bonded together. Layers can be of different materials or can be composite themselves, in order to have different properties in different directions.

2.1 Mechanics of laminated materials

2.1.1 Classical Lamination Theory

In general, the solution of elasticity problems requires a stress strain relation, which is represented by the Hooke's law:

$$\sigma = [\mathbf{C}]\epsilon \tag{2.1}$$

The vectors σ and ϵ represent respectively stress and strain and the $[\mathbf{C}]$ matrix represent the stiffness matrix. For a three-dimensional anisotropic material the stiffness matrix is a full 6x6, but because of symmetry there are only 21 independent constants, as shown in the following equation.

$$\begin{Bmatrix} \sigma_1 \\ \sigma_2 \\ \sigma_3 \\ \tau_{23} \\ \tau_{31} \\ \tau_{12} \end{Bmatrix} = \begin{bmatrix} C_{11} & C_{12} & C_{13} & C_{14} & C_{15} & C_{16} \\ C_{12} & C_{22} & C_{23} & C_{24} & C_{25} & C_{26} \\ C_{13} & C_{23} & C_{33} & C_{34} & C_{35} & C_{36} \\ C_{12} & C_{24} & C_{34} & C_{44} & C_{45} & C_{46} \\ C_{15} & C_{25} & C_{35} & C_{45} & C_{55} & C_{56} \\ C_{16} & C_{26} & C_{36} & C_{46} & C_{56} & C_{66} \end{bmatrix} \begin{Bmatrix} \epsilon_1 \\ \epsilon_2 \\ \epsilon_3 \\ \gamma_{23} \\ \gamma_{31} \\ \gamma_{12} \end{Bmatrix} \tag{2.2}$$

For an orthotropic lamina, we recall the stress-strain relation in the principal material directions:

$$\begin{Bmatrix} \sigma_1 \\ \sigma_2 \\ \sigma_3 \\ \tau_{23} \\ \tau_{31} \\ \tau_{12} \end{Bmatrix} = \begin{bmatrix} C_{11} & C_{12} & C_{13} & 0 & 0 & 0 \\ C_{12} & C_{22} & C_{23} & 0 & 0 & 0 \\ C_{13} & C_{23} & C_{33} & 0 & 0 & 0 \\ 0 & 0 & 0 & C_{44} & 0 & 0 \\ 0 & 0 & 0 & 0 & C_{55} & 0 \\ 0 & 0 & 0 & 0 & 0 & C_{66} \end{bmatrix} \begin{Bmatrix} \epsilon_1 \\ \epsilon_2 \\ \epsilon_3 \\ \gamma_{23} \\ \gamma_{31} \\ \gamma_{12} \end{Bmatrix} \tag{2.3}$$

A laminate is composed by two or more layers, perfectly bonded together so that they form one integral piece. The classical lamination theory (CLT) is founded on the following hypothesis:

- The laminate is made of orthotropic lamina bonded together, with the principal material axes of the orthotropic lamina orientated along arbitrary directions with respect to the x-y axes;
- Laminate thickness, t, is much smaller than any characteristic dimension;
- The displacements u, v, and w are small compared with t;
- In-plane strains ϵ_x, ϵ_y and γ_{xy} are small compared with unity;
- Transverse shear is negligible: $\gamma_{xz} = \gamma yz = 0$ (plane stress in each ply);
- Displacements u and v are linear functions of the thickness coordinate z (no warping);
- Transverse normal strain ϵ_z is negligible;
- Each ply obeys Hooke's Law.
- The plate thickness is constant throughout the laminate.
- Transverse shear stresse τ_{xz} and τ_{yz} vanish on the laminate surfaces.

Thus, being 1-2 the principal material plane:

$$\sigma_3 = \tau_{23} = \tau_{13} = 0 \tag{2.4}$$

Hence the stress-strain relations are reduced to:

$$\begin{Bmatrix} \sigma_1 \\ \sigma_2 \\ \tau_{12} \end{Bmatrix} = \begin{bmatrix} Q_{11} & Q_{12} & 0 \\ Q_{12} & Q_{22} & 0 \\ 0 & 0 & Q_{66} \end{bmatrix} \begin{Bmatrix} \epsilon_1 \\ \epsilon_2 \\ \gamma_{12} \end{Bmatrix} \tag{2.5}$$

where the terms Q_{ij} represent the reduced stiffenesses:

$$\begin{aligned} Q_{11} &= \frac{E_1}{1-\nu_{12}\nu_{21}}; \qquad Q_{22} = \frac{E_2}{1-\nu_{12}\nu_{21}}; \\ Q_{12} &= \frac{\nu_{12}E_2}{1-\nu_{12}\nu_{21}} = \frac{\nu_{21}E_1}{1-\nu_{12}\nu_{21}}; \\ Q_{66} &= G_{12} \end{aligned} \tag{2.6}$$

These expression are valid in the principal direction of the material, but usually, orthotropic layers are rotated with respect to a reference system. So, Eq. 2.5 must be transformed to the reference axes. In Fig. 2.2 is showed the difference between the coordinate system of the single lamina and the coordinate system of the general reference axis.

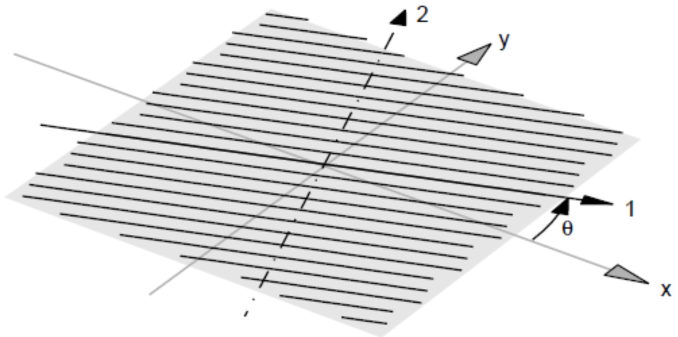

Figure 2.2

The transformation matrix is:

$$T = \begin{bmatrix} \cos^2\theta & \sin^2\theta & 2\sin\theta\cos\theta \\ \sin^2\theta & \cos^2\theta & -2\sin\theta\cos\theta \\ -\sin\theta\cos\theta & \sin\theta\cos\theta & \sin^2\theta-\cos^2\theta \end{bmatrix} \tag{2.7}$$

Furthermore, it is necessary to convert the strain vector from tensor strain notation to engineering strain notation, through the matrix R:

$$\begin{Bmatrix} \epsilon_1 \\ \epsilon_2 \\ \gamma_{12} \end{Bmatrix} = \mathbf{R} \begin{Bmatrix} \epsilon_1 \\ \epsilon_2 \\ \gamma_{12} \end{Bmatrix} \tag{2.8}$$

where:

$$\mathbf{R} = \begin{bmatrix} 1 & 0 & 0 \\ 0 & 1 & 0 \\ 0 & 0 & 2 \end{bmatrix} \tag{2.9}$$

Substituting in the stress strain relation, we obtain the following equation.

$$\begin{Bmatrix} \sigma_1 \\ \sigma_2 \\ \tau_{12} \end{Bmatrix} = \mathbf{T^{-1}QRTR^{-1}} \begin{Bmatrix} \epsilon_1 \\ \epsilon_2 \\ \gamma_{12} \end{Bmatrix} \tag{2.10}$$

As a result of the CLT hypothesis, the displacement in the x direction and in the y direction can be expressed as:

$$u = u_0 - z\frac{\partial w}{\partial x} \tag{2.11}$$

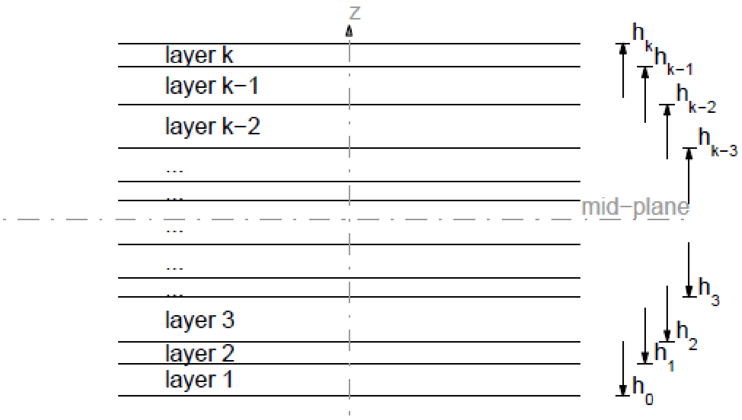

Figure 2.3

$$v = v_0 - z\frac{\partial w}{\partial y} \tag{2.12}$$

Where the subscript 0 indicates the mean surface of the laminate. In Fig. 2.3 is showed the cross section of a generic laminate, made up of different single layers.Therefore the displacements can be expressed as the following.

$$\begin{aligned} \epsilon_x &= \frac{\partial u}{\partial x} = \frac{\partial}{\partial x}(u_0 - z\frac{\partial w}{\partial x}) = \frac{\partial u_0}{\partial x} - z\frac{\partial^2 w}{\partial x^2} \\ \epsilon_y &= \frac{\partial v}{\partial y} = \frac{\partial}{\partial y}(v_0 - z\frac{\partial w}{\partial y}) = \frac{\partial v_0}{\partial y} - z\frac{\partial^2 w}{\partial y^2} \\ \gamma_{xy} &= \frac{\partial u_0}{\partial y} + \frac{\partial v_0}{\partial x} - 2z\frac{\partial^2 w}{\partial x \partial y} \end{aligned} \tag{2.13}$$

The strain distribution expressed in matrix notation is:

$$\begin{Bmatrix} \epsilon_x \\ \epsilon_y \\ \gamma_{xy} \end{Bmatrix} = \begin{Bmatrix} \epsilon_x^o \\ \epsilon_y^o \\ \gamma_{xy}^o \end{Bmatrix} + z \begin{Bmatrix} \kappa_x \\ \kappa_y \\ \kappa_{xy} \end{Bmatrix} \tag{2.14}$$

where ϵ is the vector containing the three middle strains (elongations and distortions) and κ represent the middle surface curvatures (bending curvatures and torsion).

The resultant forces and moments acting on a laminate are obtained by integration of the stresses in each layer or lamina through the laminate thickness and are defined as:

$$\begin{Bmatrix} N_x \\ N_y \\ N_{xy} \end{Bmatrix} = \int_{-h/2}^{+h/2} \begin{Bmatrix} \sigma_x \\ \sigma_y \\ \tau_{xy} \end{Bmatrix} dz \tag{2.15}$$

$$\begin{Bmatrix} M_x \\ M_y \\ M_{xy} \end{Bmatrix} = \int_{-h/2}^{+h/2} \begin{Bmatrix} \sigma_x \\ \sigma_y \\ \tau_{xy} \end{Bmatrix} zdz \tag{2.16}$$

Substituting the Eq. 2.14 for the displacements and integrating, we obtain the stress resultant and the moment resultant per unit width of the cross-section acting at a point in the laminate.

$$\begin{Bmatrix} N_x \\ N_y \\ N_{xy} \end{Bmatrix} = \begin{bmatrix} A_{11} & A_{12} & A_{16} \\ A_{21} & A_{22} & A_{26} \\ A_{36} & A_{36} & A_{36} \end{bmatrix} \begin{Bmatrix} \epsilon_x^0 \\ \epsilon_y^0 \\ \gamma_{xy}^0 \end{Bmatrix} + \begin{bmatrix} B_{11} & B_{12} & B_{16} \\ B_{21} & B_{22} & B_{26} \\ B_{36} & B_{36} & B_{36} \end{bmatrix} \begin{Bmatrix} \kappa_x \\ \kappa_y \\ \kappa_{xy} \end{Bmatrix}$$
$$\begin{Bmatrix} M_x \\ M_y \\ M_{xy} \end{Bmatrix} = \begin{bmatrix} B_{11} & B_{12} & B_{16} \\ B_{21} & B_{22} & B_{26} \\ B_{36} & B_{36} & B_{36} \end{bmatrix} \begin{Bmatrix} \epsilon_x^0 \\ \epsilon_y^0 \\ \gamma_{xy}^0 \end{Bmatrix} + \begin{bmatrix} D_{11} & D_{12} & D_{16} \\ D_{21} & D_{22} & D_{26} \\ D_{36} & D_{36} & D_{36} \end{bmatrix} \begin{Bmatrix} \kappa_x \\ \kappa_y \\ \kappa_{xy} \end{Bmatrix} \tag{2.17}$$

where:

$$\begin{aligned} A_{ij} &= \sum_1^N (\bar{Q}_{ij})_k (z_k - z_{k-1}) \\ B_{ij} &= \frac{1}{2} \sum_1^N (\bar{Q}_{ij})_k (z_k^2 - z_{k-1}^2) \\ D_{ij} &= \frac{1}{3} \sum_1^N (\bar{Q}_{ij})_k (z_k^3 - z_{k-1}^3) \end{aligned} \tag{2.18}$$

In compact format it is usually written as:

$$\begin{Bmatrix} N \\ M \end{Bmatrix} = \begin{bmatrix} A & B \\ B & D \end{bmatrix} \begin{Bmatrix} \epsilon \\ \kappa \end{Bmatrix} \tag{2.19}$$

where:

- $[A]$: extensional stiffness matrix;
- $[B]$: bending-extension coupling stiffness matrix;
- $[D]$: bending stiffness matrix.

The terms A_{ij}, B_{ij}, D_{ij} vary depending on the stacking sequence of the laminate. For instance, there are three different categories:

- Symmetric laminate $(0/\theta/\theta)_s$: $B_{ij} = 0$;
- Symmetric and balanced laminate $(0/+\theta/-\theta)_s$: $A_{16} = A_{26} = B_{ij} = 0$;
- Antimetric and balanced laminate $(0/+\theta/-\theta/+\theta/-\theta/)_s$: $A_{16} = A_{26} = D_{16} = D_{26} = B_{11} = B_{12} = B_{22} = B_{66} = 0$

2.2 Lamination parameters

The relation between Q and the rotated matrix $\bar{Q}$ can be written in a simpler notation using the material invariants, U_i, which are independent of the ply orientation. The use of material invariants, as will be seen in the following, is also useful for design optimization.

$$
\begin{aligned}
U_1 &= \frac{1}{8}(3Q_{11} + 3Q_{22} + 2Q_{12} + 4Q_{66}) \\
U_2 &= \frac{1}{2}(Q_{11} - Q_{22}) \\
U_3 &= \frac{1}{8}(Q_{11} + Q_{22} - 2Q_{12} - 4Q_{66}) \\
U_4 &= \frac{1}{8}(Q_{11} + Q_{22} + 6Q_{12} - 4Q_{66}) \\
U_5 &= \frac{1}{8}(Q_{11} + Q_{22} - 2Q_{12} + 4Q_{66})
\end{aligned}
\tag{2.20}
$$

The introduction of material invariants yields to a simpler form of the reduced stiffness matrix $\bar{Q}$:

$$
\begin{aligned}
\bar{Q}_{11} &= U_1 + U_2 \cos 2\theta + U_3 \cos 4\theta \\
\bar{Q}_{12} &= U_4 - U_3 \cos 4\theta \\
\bar{Q}_{22} &= U_1 - U_2 \cos 2\theta + U_3 \cos 4\theta \\
\bar{Q}_{16} &= \frac{1}{2} U_2 \sin 2\theta + U_3 \sin 4\theta \\
\bar{Q}_{26} &= \frac{1}{2} U_2 \sin 2\theta - U_3 \sin 4\theta \\
\bar{Q}_{66} &= U_5 - U_6 \cos 4\theta
\end{aligned}
\tag{2.21}
$$

Considering the integral form of Eq. 2.18 and assuming that all layers are of the same material, we have, for example:

$$
\begin{aligned}
&\{A_{11}, B_{11}, D_{11}\} = \int_{-h/2}^{h/2} \bar{Q}_{11}\{1, z, z^2\} dz = \\
&= U_1\{h, 0, \frac{h^3}{12}\} + U_2 \int_{-h/2}^{h/2} \cos 2\theta \{1, z, z^2\} dz + U_3 \int_{-h/2}^{h/2} \cos 4\theta \{1, z, z^2\} dz
\end{aligned}
\tag{2.22}
$$

For the other stiffness terms can be found similar equations. In order to summarize those expression we can introduce the following terms:

$$
\begin{aligned}
V_{0\{A,B,D\}} &= \int_{-h/2}^{h/2} \{1, z, z^2\} dz \\
V_{1\{A,B,D\}} &= \int_{-h/2}^{h/2} \cos 2\theta \{1, z, z^2\} dz \\
V_{2\{A,B,D\}} &= \int_{-h/2}^{h/2} \sin 2\theta \{1, z, z^2\} dz \\
V_{3\{A,B,D\}} &= \int_{-h/2}^{h/2} \cos 4\theta \{1, z, z^2\} dz \\
V_{4\{A,B,D\}} &= \int_{-h/2}^{h/2} \sin 4\theta \{1, z, z^2\} dz
\end{aligned}
\tag{2.23}
$$

In combination with material invariants matrices, lamination parameters constitute a set of variables that, along with the thicknesses, are sufficient to compute the material stiffness matrices:

$$
\begin{aligned}
\mathbf{A} &= h(\mathbf{\Gamma_0} + \mathbf{\Gamma_1} V_{1A} + \mathbf{\Gamma_2} V_{2A} + \mathbf{\Gamma_3} V_{3A} + \mathbf{\Gamma_4} V_{4A}) \\
\mathbf{B} &= \frac{h^2}{4}(\mathbf{\Gamma_1} V_{1B} + \mathbf{\Gamma_2} V_{2B} + \mathbf{\Gamma_3} V_{3B} + \mathbf{\Gamma_4} V_{4B}) \\
\mathbf{D} &= \frac{h^3}{12}(\mathbf{\Gamma_0} + \mathbf{\Gamma_1} V_{1D} + \mathbf{\Gamma_2} V_{2D} + \mathbf{\Gamma_3} V_{3D} + \mathbf{\Gamma_4} V_{4D})
\end{aligned}
\tag{2.24}
$$

From Eq. 2.24 it is possible to obtain the normalized stiffness matrices, as follows:

$$
\hat{\mathbf{A}} = \mathbf{A}\frac{1}{h}; \qquad \hat{\mathbf{B}} = \mathbf{B}\frac{4}{h^2}; \qquad \hat{\mathbf{D}} = \mathbf{D}\frac{12}{h^3}
\tag{2.25}
$$

Material invariant matrices $\mathbf{\Gamma_i}$ result from Eq. 2.20:

$$
\begin{gathered}
\mathbf{\Gamma_0} = \begin{bmatrix} U_1 & U_4 & 0 \\ U_4 & U_1 & 0 \\ 0 & 0 & U_5 \end{bmatrix}; \qquad
\mathbf{\Gamma_1} = \begin{bmatrix} U_2 & 0 & 0 \\ 0 & -U_2 & 0 \\ 0 & 0 & 0 \end{bmatrix}; \qquad
\mathbf{\Gamma_2} = \begin{bmatrix} 0 & 0 & U_2/2 \\ 0 & 0 & U_2/2 \\ U_2/2 & U_2/2 & 0 \end{bmatrix}; \\
\mathbf{\Gamma_3} = \begin{bmatrix} U_3 & -U_3 & 0 \\ -U_3 & U_3 & 0 \\ 0 & 0 & -U_3 \end{bmatrix}; \qquad
\mathbf{\Gamma_4} = \begin{bmatrix} 0 & 0 & U_3 \\ 0 & 0 & -U_3 \\ U_3 & -U_3 & 0 \end{bmatrix};
\end{gathered}
\tag{2.26}
$$

Therefore, with a set of twelve lamination parameters, is possible to completely describe a stacking sequence. In principle, lamination parameter are allowed to vary independently, but it is necessary to identify a feasible region in which they can vary in order to get a feasible stacking sequence. In the last years, many attempts have been made to obtain the exact relation for the definition of the feasible region for optimizing in-plane and bending behaviour at the same time. Some approximation can be found in Setoodeh et al.
However, Eqs. 2.24 allow us to restrict the feasible region if some geometrical constraint are defined. For example, imposing a restriction only to symmetrical laminates, the bending-extension coupling stiffness matrix vanishes and so the lamination parameters $\mathbf{V_{iB}}$.

Furthermore, if the laminate is restricted to be also balanced, also lamination parameters $\mathbf{V_{2A}}, \mathbf{V_{4A}}, \mathbf{V_{2D}}, \mathbf{V_{4D}}$ became equal to zero. As a result, when designing symmetric and balanced laminates, only four lamination parameter are sufficient to describe the stiffness properties. Further restriction applied on lamination parameters throughout the optimization design will be discussed in the following chapters.
It was shown that the stiffness properties of a generic laminate can be expressed in two different ways: it is possible to define the stacking sequence with the definition of thicknesses and orientation for each layer, or it is possible to represent the laminate with lamination parameters. The use of lamination parameters is particularly advantageous in terms of optimization, since it allows us to reduce the number of design variables.
In fact, a generic laminate can be modelled with one thickness and twelve lamination parameters, which can be further reduced with proper restrictions. On the other hand, the description of a laminate with the staking sequence requires $2n$ variables, with n being the number of layers that constitute the laminate. In industrial application it is common to have laminates with hundreds of layers, significantly increasing the number of variables.
Moreover, stiffness matrices are a linear function of continuous lamination parameters, whereas when parametrized with thicknesses and orientation, stiffness matrices are highly non-linear with respect to the defining variables.

2.2.1 Membrane stiffness visualization

In order to visualize the in-plane and out of plane stiffness distribution for a given $\mathbf{A}$ matrices, it is possible to introduce the modulus of elasticity $\hat{E}_{11}(\theta)$, with $\theta = 0°$ to $360°$, defined as:

$$\hat{E}_1 1(\theta) = \frac{1}{\hat{A}_{11}^{-1}(\theta)} \tag{2.27}$$

in which:

$$\hat{\mathbf{A}}^{-1}(\theta) = \mathbf{T^T}\hat{\mathbf{A}}^{-1}\mathbf{T}. \tag{2.28}$$

The $\hat{\mathbf{A}}$ matrix correspond to the thickness normalized stiffness matrix $\mathbf{A}$ defined previously, and $\mathbf{T}$ is the transformation matrix used in the stress-strain relationship.
From Eq. 2.27 it is possible to obtain polar stiffness distribution of the laminate. Considering a material with the properties listed in Table 2.1, it is possible to create different stacking sequences and to visualize the polar stiffness for each one of them.

E_{11}	E_{22}	G_{12}	ν_{12}	ρ
$83.0e9GPa$	$8.5e9GPa$	$4.2e9GPa$	0.35	$1452kg/m^3$

Table 2.1: Ply material properties

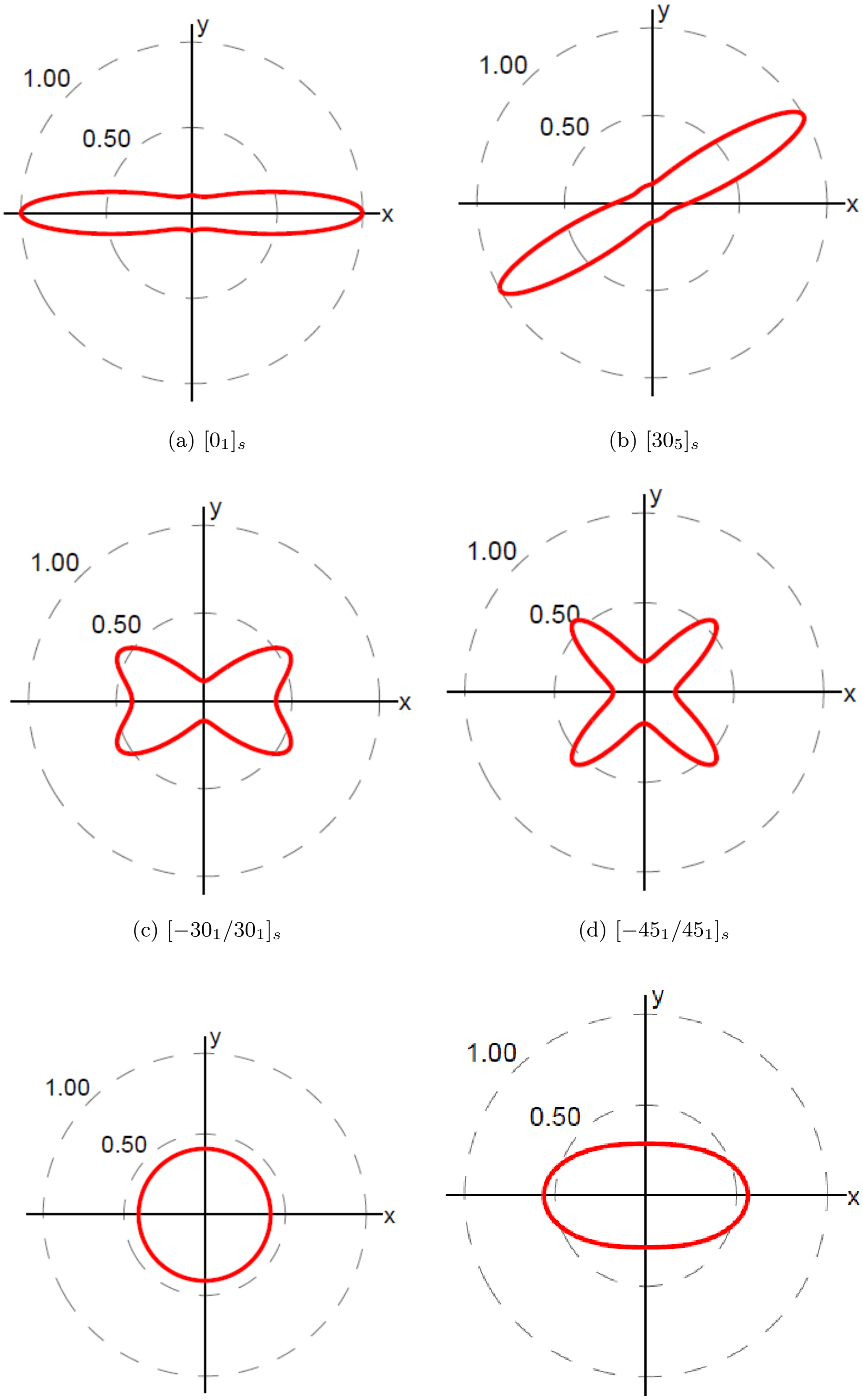

(a) $[0_1]_s$

(b) $[30_5]_s$

(c) $[-30_1/30_1]_s$

(d) $[-45_1/45_1]_s$

(e) $[-45_1/45_1/90_1/0_1]_s$

(f) $[-45_{22}/45_{22}/90_{11}/0_{44}]_s$

Figure 2.4: Polar stiffness distribution

Chapter 3

Design optimization

As said in the previous introduction, an optimization problem is characterized by an objective function, which represent the value that we want to maximize or minimize. This is done within some limits called constraints. The optimization design is driven by the changing of some values called design variables. Design variables can be continuous or discrete. In the next chapter will be shown an example where the design variable is continuous, that is the thickness of a plate. When it comes to the optimization of the stacking sequence of a laminate, for example, the design variables are, in general, discrete. The following mathematical notation is generally used to describe this problem. The design variables are described with a vector $\mathbf{x}$ with n components. The design objective is $f(\mathbf{x})$ and the constraints are $g(\mathbf{x})$ (for inequality constraints) and $h(\mathbf{x})$ (for equality constraints).
The optimization problem is, therefore, written as:

$$\begin{aligned} \textbf{minimize} \quad & f(\mathbf{x}) \qquad \mathbf{x} \in X \\ \textbf{such that} \quad & h_i(\mathbf{x}) = 0, \quad i = 1, ..., n_e; \\ & g_i(\mathbf{x}) \leq 0, \quad j = 1, ..., n_g; \\ & \mathbf{x}^L \leq \mathbf{x} \leq \mathbf{x}^U \end{aligned} \tag{3.1}$$

Where X represent the domain of the design variables, it is introduced in order to take account of the design variables that could be discrete. The upper and lower bounds of the values of the design variables are represented by $\mathbf{x}^U$ and $\mathbf{x}^L$ respectively.
For a better understanding of the problem, the following provides an example for this kind of calculation.
Minimize the objective:

$$F(\mathbf{x}) = x_1 + x_2 \tag{3.2}$$

Subject to the following constraints:

$$\begin{aligned} & g_1(\mathbf{x}) = \frac{1}{x_1} + \frac{1}{x_2} - 2 \leq 0 \\ & x_1 \geq 0.1 \quad x_2 \geq 0.1 \end{aligned} \tag{3.3}$$

In this simple example the optimal design point can be found by graphical inspection, as showed in Fig. 3.1. Usually we have more than two design variables and some non-explicit constraints and objective functions. This increases the complexity of the problem, making it necessary to use some efficient searching procedures.

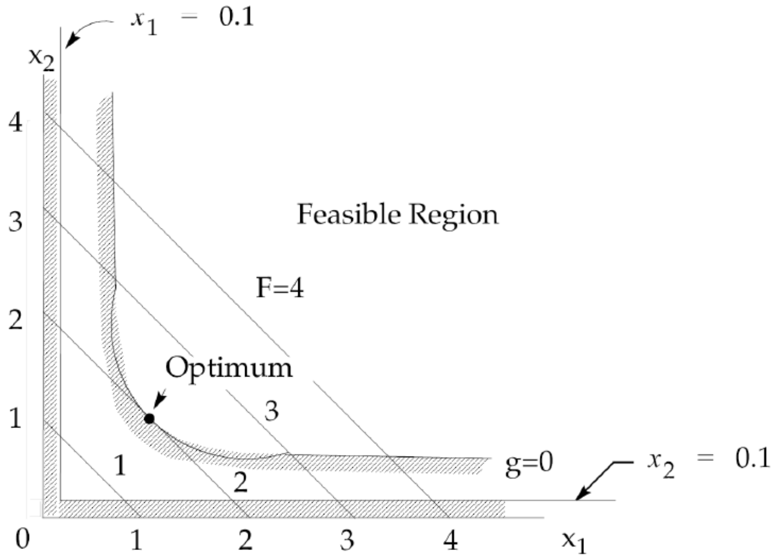

Figure 3.1

There are different algorithms that can be used to achieve the optimum design. In the following discussion is presented a short overview of the different methods available.

3.1 Gradient based optimization

The optimization algorithm used by NX Nastran belongs to the family of "gradient-based". With this kind of algorithm, in addiction to function values, function gradients are used to assist the research for the optimum.
To better understand how the gradient based optimization algorithm works, we can imagine to stand on the side of a hill and that we would like to find the point of lowest (or highest) elevation. This represent our objective function. If we also suppose that we are not able to move everywhere because some fences exist and are restricting our space, we are also representing the constraints. If we are standing inside of the fences, it is immediate to understand which point is the lowest or the highest. However, if we are blindfolded and not able to look at the hill, this is not as simple as before and further analysis are required to obtain the final decision. This is exactly the task that a numerical optimizer is faced with.
For a given point in the design space, the gradients of the objective function and of the constraints are determined and they are used to choose a direction in which to search. The optimizer will then proceed in this direction as far as possible, and repeats the process until an optimum point is found. Determining the direction to search could be complicated if the current design is infeasible or if one or more constraints are critical. Taking small steps in each of the design variable directions is the same concept of a first-forward finite difference approximation of a derivative, which is, for a single independent variable:

$$\frac{df(x)}{dx} \simeq \frac{f(x+\Delta x) - f(x)}{\Delta x} \tag{3.4}$$

Considering the whole vector of design variables, $\mathbf{x}$, we obtain the following expression:

$$\nabla F(\mathbf{x}) = \begin{Bmatrix} \dfrac{\partial F}{\partial x_1} \\ \vdots \\ \dfrac{\partial F}{\partial x_n} \end{Bmatrix} \simeq \begin{Bmatrix} \dfrac{F(\mathbf{x}+\Delta x_1) - F(\mathbf{x})}{\Delta x_1} \\ \vdots \\ \dfrac{F(\mathbf{x}+\Delta x_n) - F(\mathbf{x})}{\Delta x_n} \end{Bmatrix} \tag{3.5}$$

The gradient vector points in the direction of increasing objective function. If we want to minimize the objective function we will move in the opposite direction. So the search vector is defined as:

$$\mathbf{S} = -\nabla F \tag{3.6}$$

Once the search direction is determined, we can proceed until we reach the lowest point or a constraint. The new design at the end of the search can be written as:

$$\mathbf{x}^1 = \mathbf{x}^0 + \alpha \mathbf{S}^1 \tag{3.7}$$

With this relation we are able to reduce the dimensionality of the problem from n to 1, that is the single variable α. That is the reason for which this process is called one dimensional search. If we can no longer proceed in the search direction, this means that we reached the best design possible for that particular direction. In this situation the coefficient is called α^* and the new objective and constraint can be expressed as:

$$\begin{aligned} F^1 &= F(\mathbf{x}^0 + \alpha^* \mathbf{S}^1) \\ g_j^1 &= g_j(\mathbf{x}^0 + \alpha^* \mathbf{S}^1) \qquad j = 1, ..., n_g \end{aligned} \tag{3.8}$$

From this point in the design space we can find another search direction, proceeding until no further improvement can be made. This process will be iterated, if necessary.

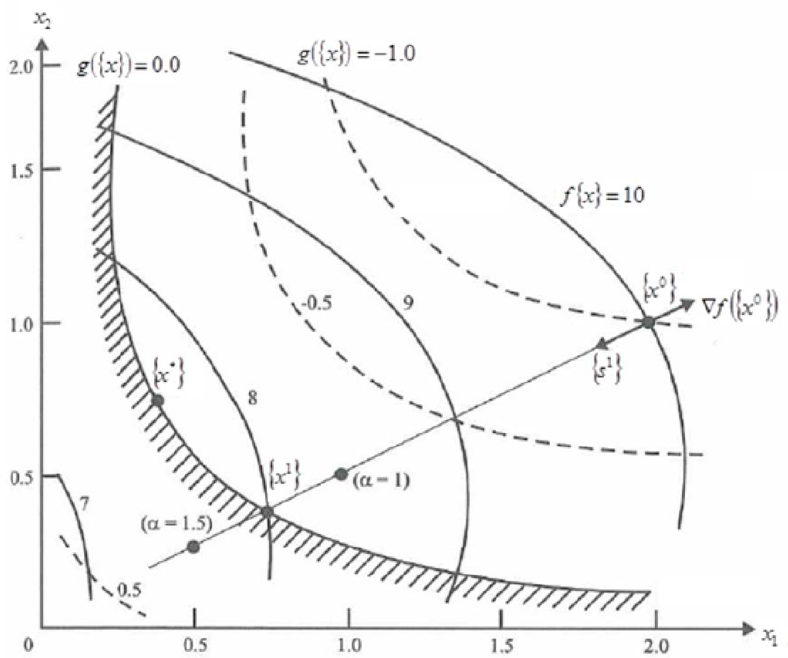

Figure 3.2

3.2 Evolutionary algorithms

In the last years evolutionary algorithms became very popular. The main difference between the classical methods (such as the gradient based) and the evolutionary algorithms is that in latter is not required any gradient information, but only a set of design points. There are two main evolutionary algorithms available: genetic algorithm (GA) and particle swarm optimization (PSO).

3.2.1 Genetic algorithm

The genetic algorithm is a method for solving both constrained and unconstrained optimization problems that, as the name may suggest, is based on Darwin's principle of survival of the fittest and the PSO is based on a simplified social model.
The genetic algorithm repeatedly modifies a population of individual solutions, selecting individuals at random from the current population to be parents and uses them to produce the children for the next generation. So, the first step in the GA is to create a random initial population. Then, the algorithm creates a sequence of new populations, using the individuals in the current generation to create the next one. In order to create the new population, the GA scores each member of the population by computing its fitness value, or *raw fitness scores*. These values are scaled in order to obtain a more usable range of values. These values are called *expectation values*. Parents are now selected, based on their expectations: the GA selects a group of individuals in the current population, the parents, who contribute their genes (the entries of their vectors) to their children. The algorithm usually selects individuals that have better fitness values as parents.

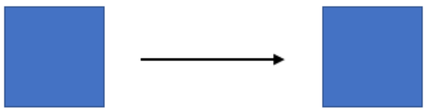

Figure 3.3: Elite child

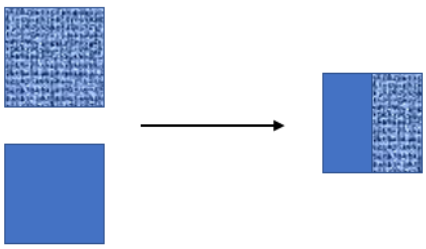

Figure 3.4: Crossover child

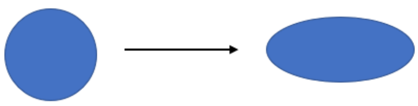

Figure 3.5: Mutation child

Three types of children are created for the next generation:

- *elite* children are the individuals in the current generation with the best fitness values. These individuals automatically survive to the next generation;
- *crossover* children are created by combining the vectors of a pair of parents;
- *mutation* children are created by introducing random changes, or mutations, to a single parent.

This process is repeated, so that the population can evolve toward an optimal solution, until one of the stopping criteria is met or convergence is achieved.
Unlike other search algorithms that move from one point to another, such as the gradient based algorithm, GAs work with a population of strings, increasing the chances of obtaining global or near-global optima. Furthermore, working with a population of designs also allows the implementation of parallel computing, reducing the time needed for the optimization analysis.
Another advantage resulting from the use of genetic algorithms is that the outcome of the search is random, so repeated optimization can yield to different designs, which can be useful when dealing with a design space with many local optima.

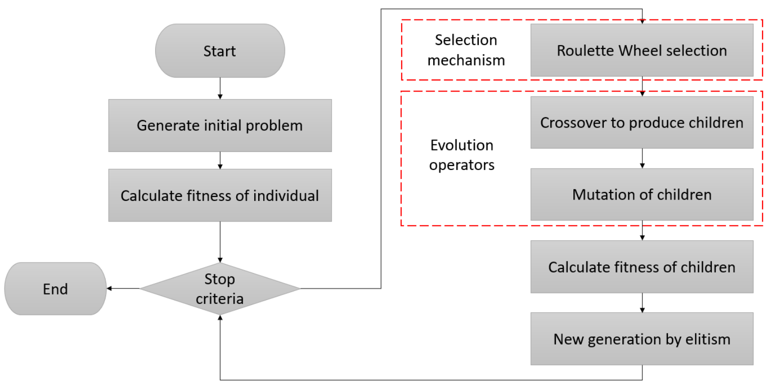

Figure 3.6: Genetic algorithm flowchart

3.2.2 Particle Swarm Optimization

The particle swarm optimization is based on the behaviour of a swarm searching for food. A collection of individuals called particles move in steps throughout a region. At each step, the algorithm evaluates the objective function at each particle. After this evaluation, the algorithm decides on the new velocity of each particle. The particles move, then the algorithm reevaluates. Each particle is attracted to some degree to the best location it has found so far, and also to the best location any member of the swarm has found. After some steps, the population can coalesce around one location, or can coalesce around a few locations, or can continue to move. The population converges on the optimum design using information gained both from each individual and from the swarm as a whole.

Chapter 4

Aeroelastic tailoring

As stated in the previous chapters, weight minimization is one of the primary goals in aerospace industry. However, the real objective for the design of an aircraft, is performance, which may involve weight as a constraint, but also payload, range, and others. Aeroelastic tailoring is a way of maximizing measures of performance. Furthermore, it involves the use of structural deformation of a lifting surface to achieve aircraft performance objective which are not usually associated with structural design. Therefore, aeroelastic tailoring can be defined as following:
Aeroelastic tailoring is the embodiement of directional stiffness into an aircraft structural design to control aeroelastic deformation, static or dynamic, in such a fashion as to affect the aerodynamic and structural performance of that aircraft in a beneficial way.
Aeroelastic tailoring is not a new concept, since it was applied by Munk in a wooden propeller design in 1949. In Munk's design, fiber orientation of the wood is optimized in order to obtain a beneficial deformation of the propeller as the load increases. The most recent application of aeroelastic tailoring is on the X-29 demonstrator aircraft. It is known that forward-swept wings present some benefits mainly down to manoeuvrability. In fact, they maintain airflow over their surfaces at steeper climb angles than conventional planes, which means the nose can point higher without the aircraft going into a dangerous stall. However, they present an important issue with aeroelastic divergence. In a forward-swept wing configuration, the aerodynamic lift causes a twisting force that rotates the leading edge upward, causing a higher angle of attack, which in turn increases lift, and twists the wing further. With conventional metallic construction, additional torsional stiffening is typically required which adds weight, and is therefore sub-optimal in terms of aircraft performance.
In order to avoid divergence, advanced composite materials and aeroelastic tailoring can be used. For instance, considering a layer of continuos fibre-reinforced composite, if the fibres are aligned at an angle to the x-direction (θ), and a load is applied in the x-direction, then the layer will not only stretch in the x-direction and compress in the y-direction but also shear. This is because the layer will stretch less in the fibre direction than in the resin direction. This behaviour can be avoided if the number of layers oriented at $+\theta$ are balanced with the same number of layers oriented at $-\theta$, forming a stacking sequence such as $[-\theta/+\theta/+\theta/-\theta]$. However, this stacking sequence will present a bend-twist coupling, because the bending stiffness of a layer is a factor of the layer-thickness cubed plus the

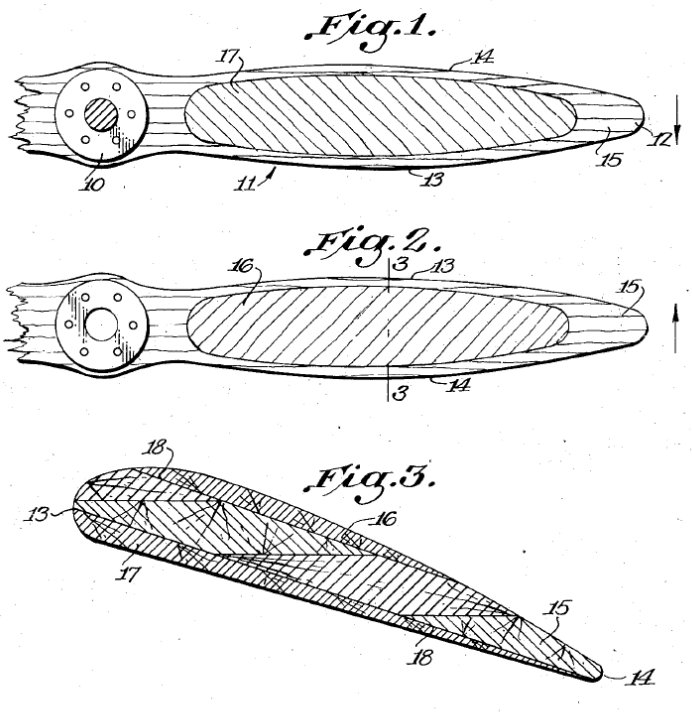

Figure 4.1: Munk's propeller design

distance from the axis of bending (here the mid-plane) squared. Thus, even if the $+\theta$ and $-\theta$ layers have the same thickness, the outer $+\theta$ layers contribute more to the bending stiffness of the laminate than the $-\theta$ layers do. Therefore, stretching-shearing coupling is eliminated in a $[-\theta/+\theta/+\theta/-\theta]$ laminate as the number of $+\theta$ and $-\theta$ layers is the same, but bend-twist coupling will occur because the $+\theta$ layers are further from the mid-plane than the $-\theta$ layers.

Figure 4.2: X-29 forward-swept wing demonstrator aircraft

4.1 Optimization strategy

As mentioned previously, for the purpose of optimization, it is not convenient to directly use the stacking sequence for optimization design, instead, lamination parameters are going to be used. The optimization design strategy adopted in the present dissertation is divided in two steps. The first step of optimization concerns the lamination parameters of the laminate. In this step, called *continuous optimization*, lamination parameters are optimized with a gradient based algorithm, applying all the physical multidisciplinary constraints. The second step, called *discrete optimization*, refers to the retrieving of the stacking sequence, using a genetic algorithm.

4.1.1 Continuous optimization constraints

Feasibility constraints

Nowadays, the explicit expression relating all the 12 lamination parameters are still unknown. In order to determine the design space for lamination parameters, Diacoun et al. [6] developed a method based on variational approach. The feasible region is numerically obtained determining the layup function $\theta(z)$ which maximizes:

$$\begin{aligned} F(\theta(z)) =& k_1^A V_{1A} + k_2^A V_{2A} + k_3^A V_{3A} + k_4^A V_{4A} + k_1^B V_{1B} + k_2^B V_{2B} + \\ &+ k_3^B V_{3B} + k_4^B V_{4B} + k_1^D V_{1D} + k_2^D V_{2D} + k_3^D V_{3D} + k_4^D V_{4D} \end{aligned} \tag{4.1}$$

The functional F results constant on an hyperplane of which unit normal is:

$$\mathbf{k} = \{k_1^A, ...k_4^D\} \tag{4.2}$$

and the boundary of the design space for lamination parameters is found at maximum F for a given $\mathbf{k}$. Explicit relations relating the lamination parameters can be obtained:

$$\begin{aligned} & V_{1B}^2 + V_{3B}^2 \leq 1 \\ & V_{2B}^2 + V_{4B}^2 \leq 1 \\ & V_{2B} \leq 4\left(V_{1B} - V_{1B}^2\right) && for && V_{1B} \geq \frac{1}{2} \\ & V_{2B} \leq 4\left(V_{3B} - V_{3B}^2\right) && for && V_{3B} \geq \frac{1}{2} \\ & V_{4B} \leq 2V_{1B}\sqrt{1 - V_{1B}^2} && for && V_{1B} \geq \frac{\sqrt{2}}{2} \\ & V_{4B} \leq 2V_{3B}\sqrt{1 - V_{3B}^2} && for && V_{3B} \geq \frac{\sqrt{2}}{2} \\ & 4(V_{iD} - 1)(V_{iA} - 1) \geq (V_{iA} - 1)^4 + 3V_{iB}^2 \\ & 4(V_{iD} + 1)(V_{iA} + 1) \geq (V_{iA} + 1)^4 + 3V_{iB}^2 \end{aligned} \tag{4.3}$$

For symmetrical laminates, the feasibility constraint to impose are the following and were analytically obtained by Fukunaga and Sekine [7]:

$$
\begin{aligned}
&2(V_{1A})^2 - 1 \le V_{2A} \le 1 - (V_{3A})^2 \\
&2(1 + V_{2A})(V_{3A})^2 - 4V_{1A}V_{3A}V_{4A} + (V_{4A})^2 \le [V_{2A} - 2(V_{1A})^2 + 1](1 - V_{2A}) \\
&2(V_{1D})^2 - 1 \le V_{2D} \le 1 - (V_{3D})^2 \\
&2(1 + V_{2D})(V_{3D})^2 - 4V_{1D}V_{3D}V_{4D} + (V_{4D})^2 \le [V_{2D} - 2(V_{1D})^2 + 1](1 - V_{2D})
\end{aligned}
\tag{4.4}
$$

Those equation are restraining the space of solution for lamination parameters, in the following figures are showed some examples for the new feasible region after applying those constraints.

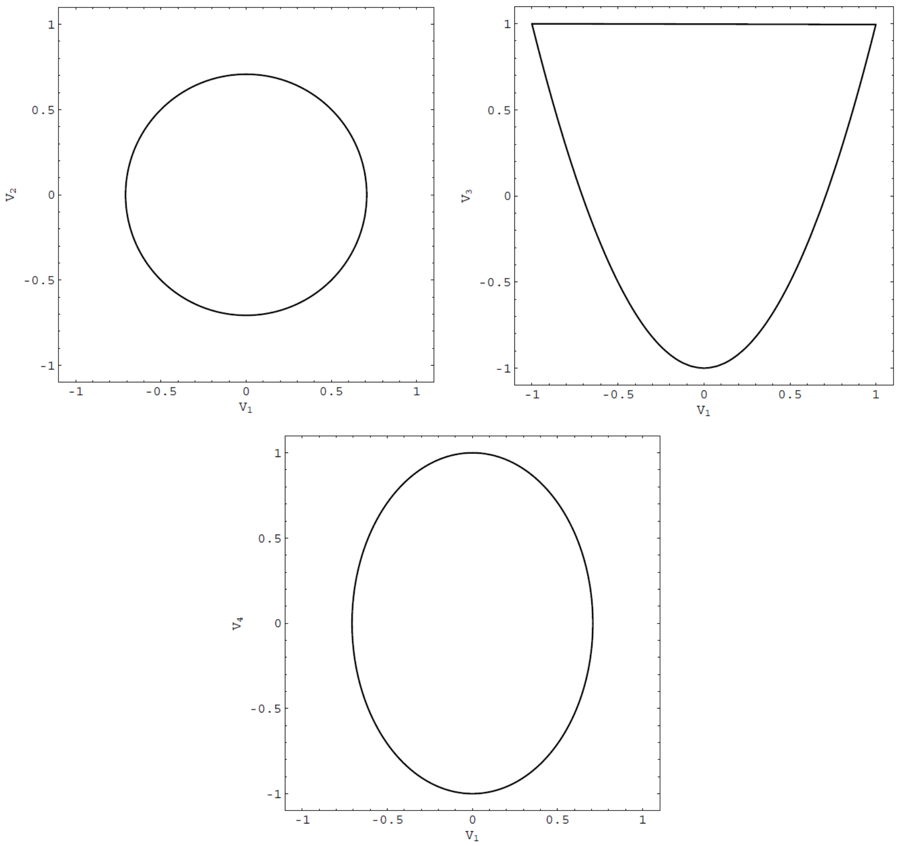

Figure 4.3

Physical constraints

When it comes to optimizing a structure, it is clearly not sufficient to constraint the new configuration only with theoretical feasibility constraints. It is necessary to translate into mathematical constraints every structural design requirements, such as strength, stiffness or stability constraints.

In order to fulfil the requirements, for each iteration different kind of analysis will be made by the optimizer, according to the design responses to be constrained. Typically, the responses are strains, displacement and eigenvalues from static, buckling and flutter analysis.

One of the most critical issues in laminate composite material design is the prediction of failure. This is usually obtained by comparing stresses or strains computed in the model with the allowable of the material. For laminate materials there are additional levels of complexity with respect to isotropic materials. In the first place, composite material are usually characterized by brittle failure, which is less tolerated than the failure that happens in ductile materials. In fact, for ductile materials the failure is in form of yielding and usually remains localized. Furthermore, the failure of a laminate is strongly influenced by the stacking sequence of the material. Stresses and strengths may be different in layers, hence it is possible that one of the layers reaches their limit earlier than the others, therefore the layer would suffer of brittle failure. That is a form of localized failure for the laminate, preceding the total failure of the material.
In application where this kind of failure is not acceptable, failure prediction on the first failure is commonly referred as first-ply failure criterion.

Failure index is one of the physical constraints that usually found in design optimization. Since the staking sequence of the laminate is no longer available when optimizing lamination parameters, it is necessary to determine a conservative failure envelope, such that every possible stacking sequence will present no failure. One of the failure criteria that can be developed is based on the Tsai-Wu criterion:

$$F_{11}\sigma_1^2 + F_{22}\sigma_2^2 + F_{66}\tau_{12}^2 + F_1\sigma_1 + F_2\sigma_2 + 2F_{12}\sigma_1\sigma_2 = 1 \tag{4.5}$$

in which the second and fourth order tensors of strength are given by the following expressions:

$$\begin{aligned} &F_{11} = \frac{1}{X_t X_c}; \qquad F_{22} = \frac{1}{Y_t Y_c}; \qquad F_{12} = \frac{-1}{2\sqrt{X_t X_c Y_t Y_c}}; \\ &F_1 = \frac{1}{X_t} - \frac{1}{X_c}; \qquad F_2 = \frac{1}{Y_t} - \frac{1}{Y_c}; \qquad F_{66} = 1/S^2 \end{aligned} \tag{4.6}$$

where X_t, X_c, Y_t, Y_c are tensile and compressive failure stresses of x and y direction, respectively, and S is the shear failure stress.

Manufacturing and blending constraints

Even though the theoretical expressions for lamination parameters allow us to use generic angles, in real industrial application, this is not possible. Usually, during the manufacturing process, only specific orientations can be used, yielding to new constraints.
Standard angles in manufacturing are: $\pm 45°, 0°, 90°$. Recalling Eq. 2.23 it can be seen that using only this values for θ, lamination parameters V_{4A} and V_{4D} vanish.
However, considering this limitation on the stacking sequence is not sufficient. We must also take into account that neighbouring patches share a number of common plies, introducing the blending constraints. Usually, this kind of constraint is implemented in the second step of the optimization, which is the discrete optimization, though running a lightly constrained first step optimization and then a highly constrained discrete stacking sequence retrieval

can result in high discrepancies between the two analysis. Therefore it is necessary to introduce the blending constraints also in the continuous optimization with lamination parameters, in order to get a more significant solution.
There are different blending rules that have been defined in the past decades, such as blending rules that consider only the outer or the inner layers, or generalized blending, where plies are dropped also between the inner and the outer ply. In Fig. 4.4 and 4.5 the two different type of blending are showed.

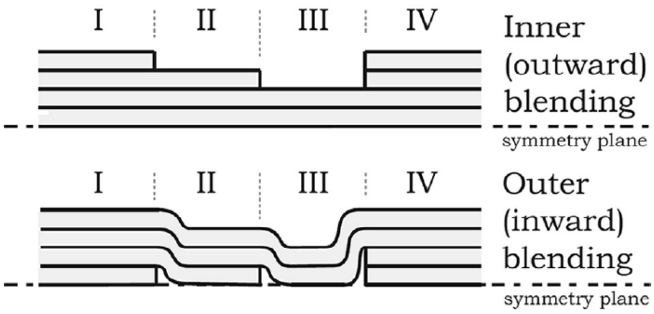

Figure 4.4

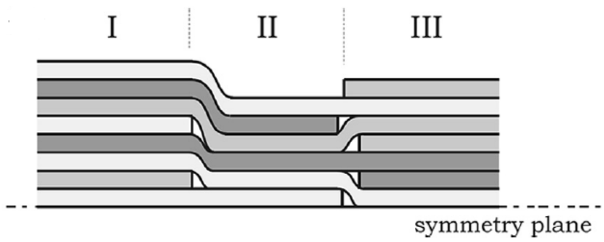

Figure 4.5

The derivation of the blending constraints in lamination parameters space comes from Eq. . The fundamental idea behind the blending constraint is evaluating the change in lamination parameters due to ply-drops. For example, the change in the lamination parameter V_1^A due to one ply drop can be quantified as following. With $V_{1(N-1)}^A$ we denote the value of V_1^A after one ply drop:

$$V_{1(N-1)}^A = \frac{1}{N-1} \sum_{i=1}^{N} cos(2\theta_i) \tag{4.7}$$

so, the difference between V_1^A before and after one ply drop is:

$$V_{1(N)\to(N-1)}^A = V_{1(N)}^A - V_{1(N-1)}^A = \frac{1}{N} cos(2\theta_j) + \left(\frac{1}{N} - \frac{1}{N-1} \right) \sum_{i=1}^{N} cos(2\theta_i) \tag{4.8}$$

The maximum of the function is:

$$max||V_{1(N)\to(N-1)}^A|| = \frac{2}{N} \tag{4.9}$$

Generalizing to any number X of ply drops:

$$max||V^A_{1(N)\to(N-1)}|| = 2\frac{X}{N} \tag{4.10}$$

Carrying out the corresponding calculations for the remaining lamination paramters, can be seen that $2(X/N)$ is always the maximal magnitude, so the blending constraint can be set as follows:

$$||\Delta V^A_{k(N)\to(N-X)}|| \leq 2(X/N), \qquad fork = 1{,}2{,}3{,}4 \tag{4.11}$$

Similarly, also the out of plane blending constraint can be obtained. In summary, the blending constraint can be defined as:

$$\begin{aligned} &||\Delta V^A_{1,2,3,4}||^2 - \alpha(\frac{T_i - T_j}{max(T_i,T_j)})^2 \leq 0 \\ &||\Delta V^D_{1,2,3,4}||^2 - \beta(3\left[\frac{T_i - T_j}{max(T_i,T_j)}\right] - \left[\frac{T_i - T_j}{max(T_i,T_j)}\right]^2 + 4\left[\frac{T_i - T_j}{max(T_i,T_j)}\right]^3)^2 \leq 2 \end{aligned} \tag{4.12}$$

Chapter 5

Preliminary assessment

In the following chapter will be shown some examples of design optimization performed with Femap and NX Nastran.
Femap (Finite Element Modeling And Post-processing) is a pre- and post-processor developed to be able to handle different solvers such as Abaqus, NX Nastran, etc. Throughout this dissertation the optimization tool, among all, will be most widely used. It allows to perform optimization analysis in order to minimize the weight of a certain component, modifying the main characteristics of rods, bars and plates elements. Limits can be setted for several kind of responses, such as stress, strain, displacement or frequency. Moreover, optimization analysis can be enhanced through add-on tools and APIs. In section 5.1 will be performed a static analysis, optimizing the weight of a plate constraining the maximum Von Mises stress. In section 5.2 will be performed a normal modes analysis, constraining the fundamental natural frequency.

5.1 Static analysis

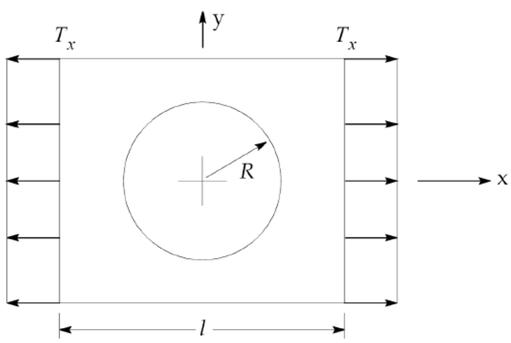

Figure 5.1

The subject of the study is an aluminium plate subject to uniform tensile stress as shown in Figure 5.1. The objective of the optimization design is to minimize the weight of the plate, modifying its thickness.

The plate has the following geometrical characteristics: $l = 100\,mm$, $R = 10mm$, $t = 5\,mm$ and it is loaded with $T_x = 50\,N$. Aluminium properties are given in Table 5.1.
The first step is to run a static analysis in order to know how the stress is distributed on the plate.

$E[MPa]$	ν	$\rho[kg/mm^3]$	$\sigma_{max}[MPa]$
73000	0.33	2.7e-6	400

Table 5.1: Aluminium properties

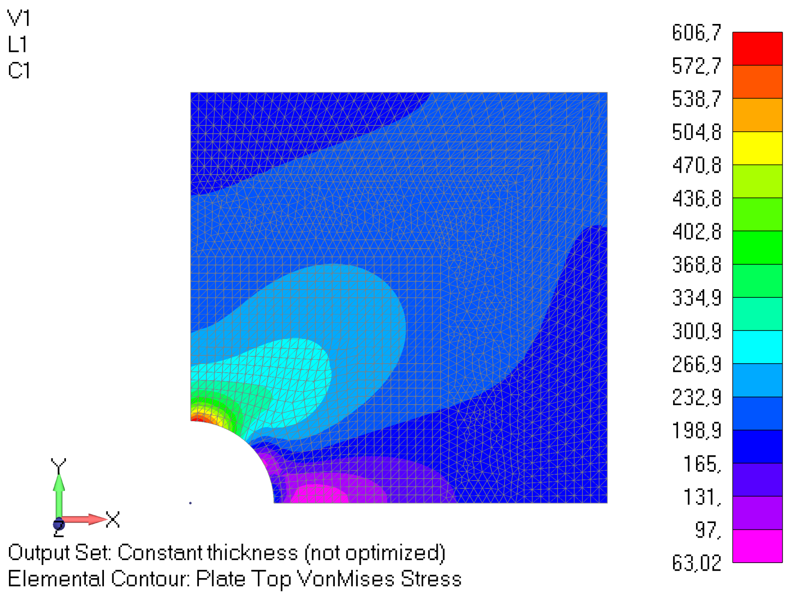

Figure 5.2: Von Mises stress distribution

In Figure 5.2 is shown the stress distribution on the plate. Stress around the hole is too high, above the σ_{max} of aluminium, while it decreases moving towards the extremes of the plates. In order to avoid breaking the plate we can adjust the thickness using Femap Optimization Analysis.
The ideal solution would be to reach σ_{max} on every point of the plate. This solution is not simple to achieve, especially because it would depend on the mesh quality.
There will be shown two different solution: in the first case the plate thickness will vary remaining constant all over the plate, in the second case the plate will be divided in 8 parts with different thickness.

5.1.1 Constant thickness

In the first case the optimizer will vary the plate thickness in order to avoid breaking the plate. Initial thickness is set to be $t_i = 5mm$, consequently the weight of the plate is $W_i = 0.033\,kg$. Plate thickness, t, is the design variable and will vary between a minimum and a maximum value:

$$1\,mm < t < 10\,mm$$

Von Mises stress value will be the design constraint:

$$10\,MPa < \sigma < 400\,MPa$$

In Table 5.2 the optimization analysis results are compared with initial values and in Figure 5.3 is shown the new Von Mises stress distribution.

	$t\,[mm]$	$W\,[kg]$
Initial	5	0.033
Final	8.26	0.054

Table 5.2: Optimization analysis results.

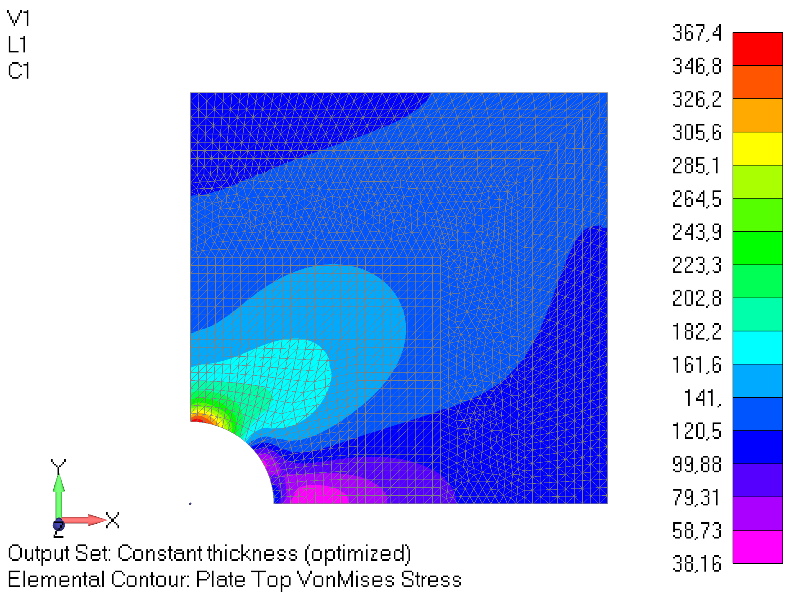

Figure 5.3: Von Mises stress distribution (optimized plate)

In order to ensure $\sigma < \sigma_{max}$ all over the plate the only possible solution is to increase the whole thickness. It can be noticed that stress distribution is the same as the previous analysis, the only difference are the stress values. As mentioned above, this is not the best solution. A large amount of material is redundant: blue and pink regions are far below the maximum allowable stress, meaning that in those regions the plate could be thinner. In the following figures are reported the design variables and design objective variation with respect to the number of iterations.

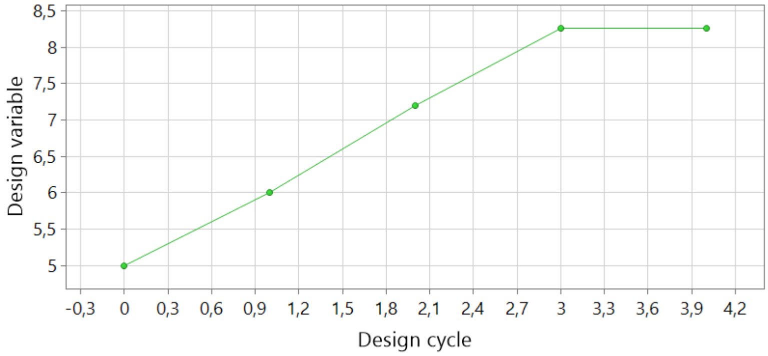

Figure 5.4

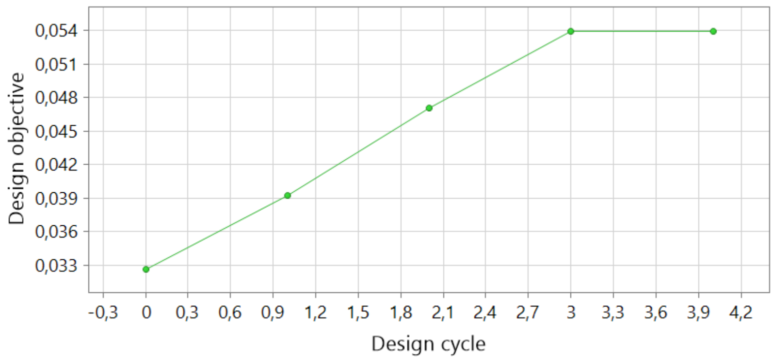

Figure 5.5

5.1.2 Variable thickness

In order to obtain a more refined result, in this case the plate is divided in 8 different sections. The optimizer will vary every zone's thickness independently: in this case there are 8 design variables and 8 design constraint. As introduced in the previous analysis, thicknesses may vary between 1 mm and 10 mm and in every section maximum stress shall not exceed σ_{max}. In Figure 5.6 is shown section enumeration.

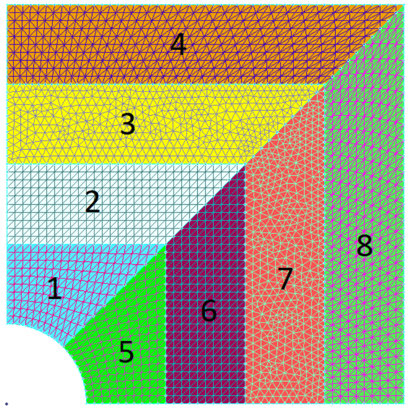

Figure 5.6: Section enumeration

Optimization analysis results are given in Table 5.3, compared with initial values. As expected, thickness of sections 3, 4, 7 and 8 decreased significantly, while thickness of section 1, where in the first analysis $\sigma > \sigma_{max}$, increased, almost doubling its initial value.

	t_1	t_2	t_3	t_4	t_5	t_6	t_7	t_8	$W\ [kg]$
Initial	5	5	5	5	5	5	5	5	0.033
Final	9.29	4.13	2.93	2.51	3.99	3.97	2.77	2.69	0.023

Table 5.3: Optimization analysis results. All length are expressed in $[mm]$.

In Figure 5.7 is shown the new Von Mises stress distribution. Comparing those results with the previous analysis' results (Figure 5.3) it can be noticed that the material is distributed in a more efficient way. In fact, stress value near the plate's edges is now almost equal to aluminium maximum allowable stress. Despite this improvement, there are discontinuities in stress distributions on the edge of each region. This is due to the new thickness distribution over the plate, which is represented in Figure 5.8. This suggest that further optimization could be reached by smoothing those edges, in order to avoid an eventual notch effect. Moreover, additional optimization could be done in the region near the hole, where there are still some elements where stress is far less than σ_{max}.
In Figure 5.9 is shown the design variables trend with respect to the number of iteration needed.

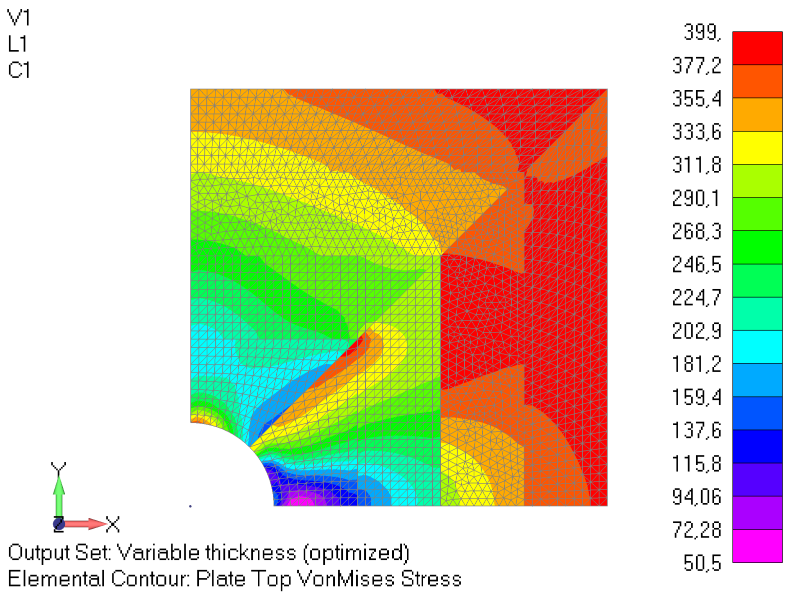

Figure 5.7: Von Mises stress (optimized plate)

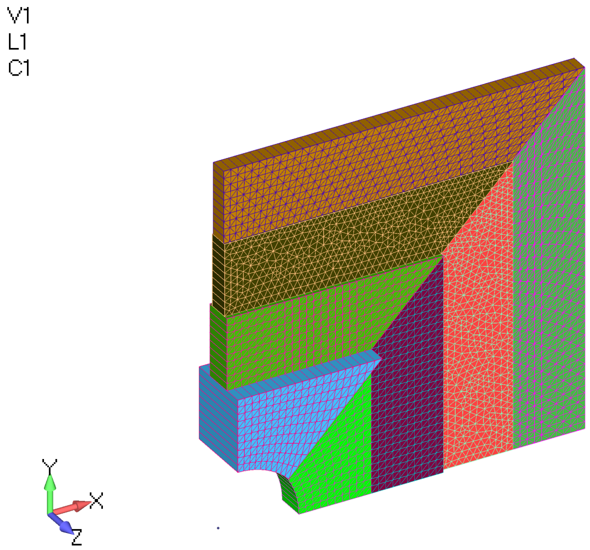

Figure 5.8

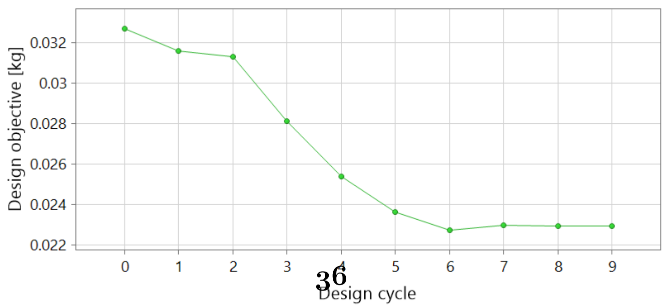

Figure 5.10: Weight vs number of iteration

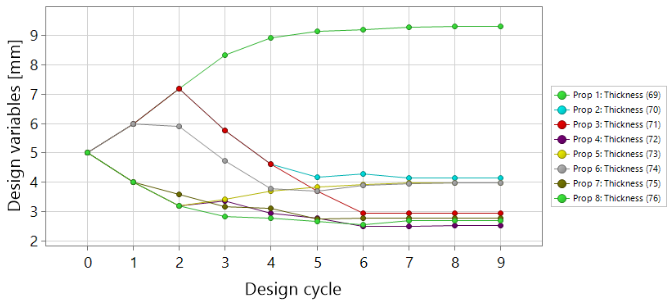

Figure 5.9: Thickness variation vs number of iteration

Variable element-wise thickness

Figure 5.11

As previously said, the best solution is to vary every elemental thickness in order to find the value that provides σ_{max} on every mesh element. This solution is extremely influenced by the quality of the mesh. The model used for this kind of analysis is showed in Figure 5.11. In order to minimise the execution time of the optimization analysis, has been used a mesh with fewer elements.
Through the use of an API has been possible to assign to each element a different property in order to individually vary the elements thicknesses. Therefore, having 233 elements, there are now 233 design variables and design constraints. The design objective remains the same.
It has to be said, however, that not only the mesh quality influences the outcome of the analysis, but also the initial conditions. This is a characteristic of gradient-based algorithm, in fact, due to the nature of the method, the optimizer won't be able to find the

global minimum, but only a local one. So, according to the initial conditions, optimization analysis could lead to different results, or, in worst case scenario, could not converge at all. In there circumstances, setting the initial thickness of the plate to $t = 5$ causes the analysis to diverge.
The optimization analysis converges if the initial thickness is set to $t = 4mm$. Stress distribution after optimizing the elements thicknesses is showed in Figure 5.12. In this case stress distribution is almost constant and equal to the maximum allowable stress of aluminium, except on the elements near the hole. In the following table is shown the comparison between the optimized weight obtained in the three previous cases. In Figure 5.13 is showed the updated geometry of the plate after being optimized.

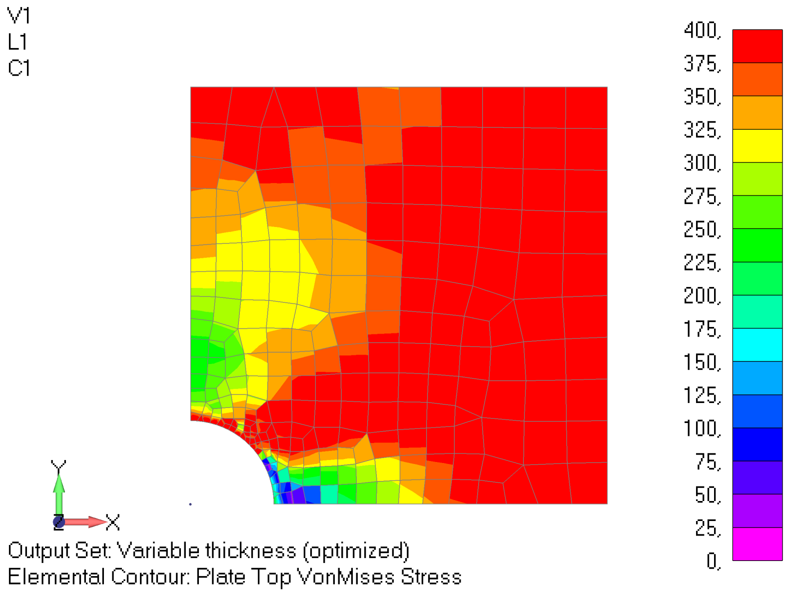

Figure 5.12

	Weight
Initial ($t = 5mm$)	$0.033\,kg$
Constant thickness	$0.054\,kg$
Variable thickness (1)	$0.023\,kg$
Variable thickness (2)	$0.020\,kg$

As expected, it may be concluded that the best solution to optimize the weight of the plate is to vary every element thickness, while the worst is to keep the thickness constant on the whole plate. Of course, the three cases showed are merely an example of the various ways that could be used to optimize the weight of an object. Indeed, there are other aspects to be considered, such as technological issues. For example, the last solution was established to be the best one, but, on the other hand, it would be hard to manufacture a piece with such characteristics. So it could be easier and cheaper to chose the first solution, where the plate won't break but will be heavier.

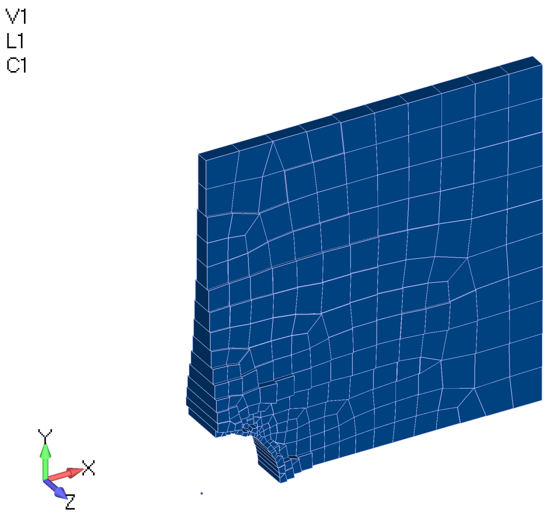

Figure 5.13

5.2 Normal modes analysis

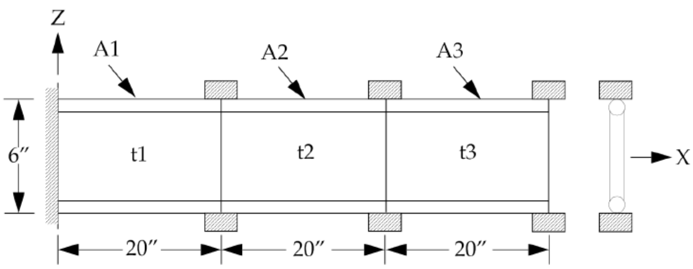

Figure 5.14: Cantilevered beam

In the following example there will be shown the optimization design of a cantilevered beam with specified natural frequencies. This is known also as "Turner's problem", since it was originally published by Turner's. The objective of the study is to minimize the mass structure of the beam showed in Figure 5.14 while constraining the fundamental natural frequency at or above 20 Hz.
Geometrical characteristics are the following: $a = 6\,in$, $b = 20\,in$, $t_1 = t_2 = t_3 = 0.2\,in$, $A_1 = A_2 = A_3 = 1\,in^2$. There are also lumped masses at top and bottom nodes, $16 lbs$ each. The whole structure is made of aluminium, which properties were reported in Table 5.1.
With initial proprieties the first natural frequency is $f_i = 24.9 Hz$. The corresponding deformed structure is shown in Figure 5.15.

There are six different design variables: three for the different web thicknesses and three for the rod cross-sectional areas. After running the optimization design the first natural

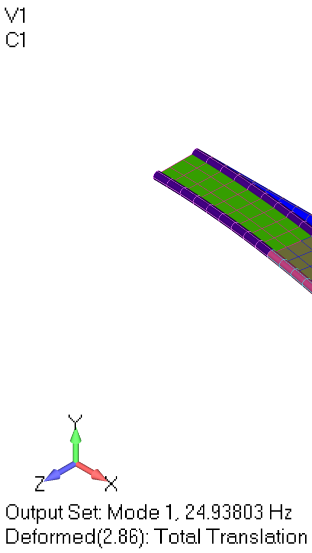

Figure 5.15

frequency computed is $f_f = 19.9Hz$ and the updated design variables are shown in Table 5.4.

	$t_1\,[in]$	$t_2\,[in]$	$t_3\,[in]$	$A_1\,[in^2]$	$A_2\,[in^2]$	$A_3\,[in^2]$	$W[lb]$
Initial	0.2	0.2	0.2	1	1	1	115.2
Final	0.049	0.044	0.027	0.94	0.48	0.16	103.8

Table 5.4: Optimization analysis results.

In Figure 5.16 is shown a comparison between the initial model (on the left) and the model with the updated thicknesses and areas (on the right).

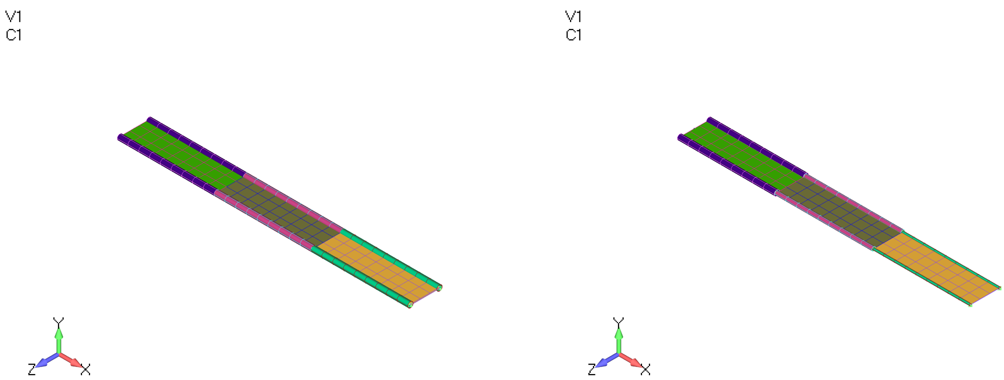

Figure 5.16

In Figures ??, 5.18 and 5.19 is shown the trend of the design variables and of the design objective with respect to the number of iteration.

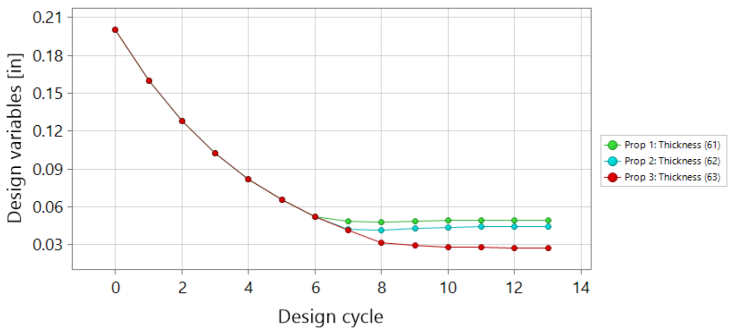

Figure 5.17

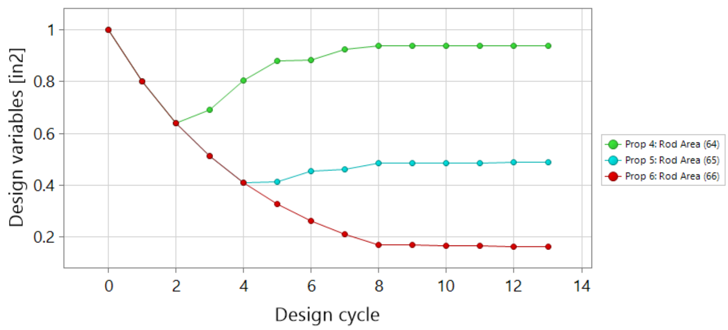

Figure 5.18

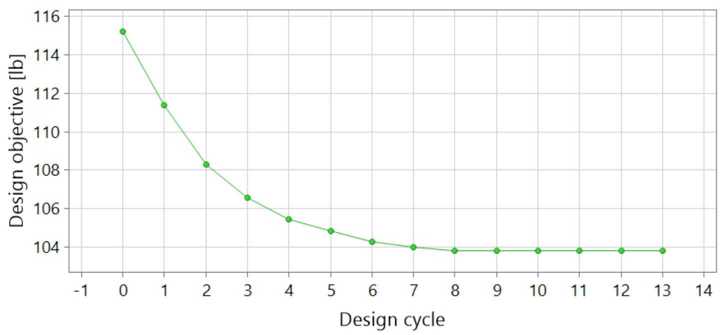

Figure 5.19

5.2.1 Buckling analysis of a laminated plate

In the following example a laminated plate subject to compressive load is optimized. In Fig. 5.20 are showed the loading and the constraint of the problem.

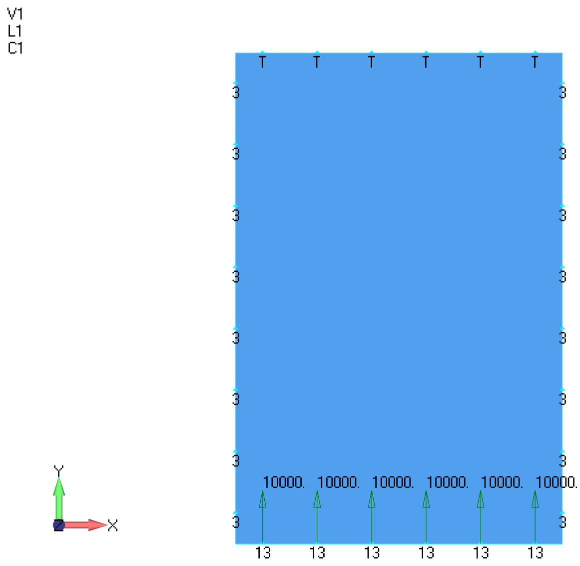

Figure 5.20

The design objective of this example is, as previously, the weight minimization. However, unlike the previous examples, the plate is made of a laminate composite, so that it is possible to have new design variables. In this particular case, the laminate is composed of three laminae, so a total of six design variables are defined: three comes from the thicknesses and three from the orientations. In this analysis both the first buckling eigenvalue and the failure index are constrained. Furthermore, it is possible to consider also some manufacturing constraint for the orientation of the layers, making the design variables concerning the orientations no longer continuous but discrete. In summary, the present problem is defined by:

- 1 design objective: weight minimization;
- 6 design variables:
  - 3 ply orientations: $-90° \leq \theta \leq 90°; \quad \Delta\theta = 15°$
  - 3 ply thicknesses
- 2 constraints:
  - Failure index ≤ 1
  - First buckling eigenvalue: $1 \leq \lambda_1 \leq 1.5$

Initial conditions

Initial condition of the problem are characterized by the following values for weight, first buckling eigenvalue and failure index:

$$W_i = 0.0578kg$$
$$\lambda_{1i} = 10.6$$
$$FI_i = 2.03$$

In Fig. 5.21 are showed the failure index and the first buckling mode of the plate.

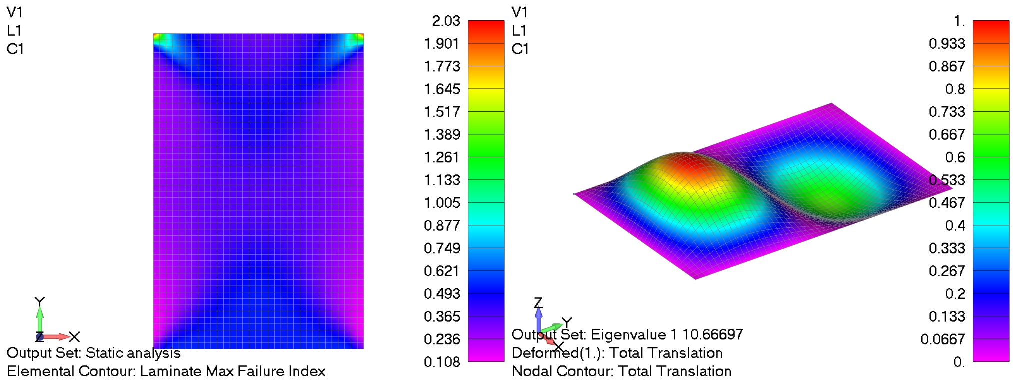

(a) Failure index (b) First buckling mode

Figure 5.21

The initial stacking sequence is $[-30°/0°/30°]$ as showed in Fig. 5.22

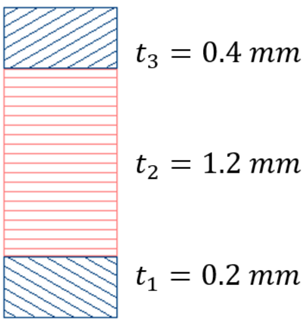

Figure 5.22

It can be seen that initially, neither the failure index nor the eigenvalue constraint are satisfied. During the optimization a gradient based algorithm will change the layers thicknesses and orientation in order to get an optimum solution that fulfils the indicated constraints.

Final conditions

After running the optimization, the following results are obtained:

$$W_i = 0.0435kg$$
$$\lambda_{1i} = 1.03$$
$$FI_i = 0.801$$

New failure index and buckling mode are showed in Fig. 5.23.

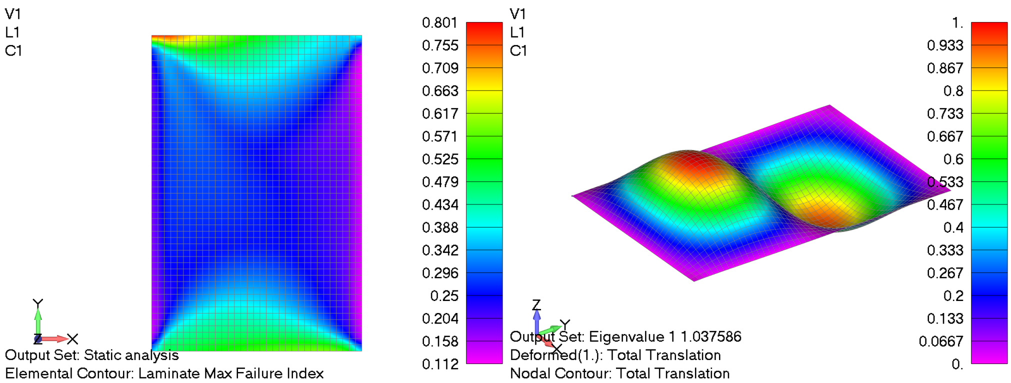

(a) Failure index (b) First buckling mode

Figure 5.23

The new stacking sequence obtained is $[-15°/0°/30°]$ as showed in Fig. 5.24.

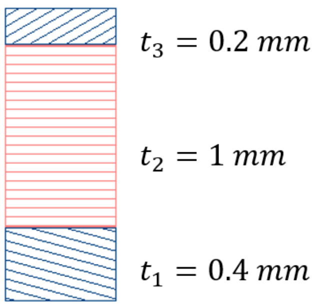

Figure 5.24

Chapter 6

CFM Dardo wing model

The present work is part of the Aeroelastic Tailoring project headed by Embraer S.A. The Aeroelasting Tailoring group involves more than ten International partners, whose aim is to develop a framework of processes and tools to navigate structural design drivers of an aircraft satisfying multiple physical requirements (structures, loads, flutter, and performance) and to provide insight on how new technologies may affect aircraft design with particular reference to composite materials.
The project is focused on optimization, manufacturing and testing of a composite wing for an aircraft that can be representative for the assessment of Embraer Aeroelastic Tailoring framework. In the following chapter will be presented the model of the current wing and the analysis simulations result obtained with FEMAP, which represent the basis for the future optimization.

6.1 FEM model

The project is focused on a specific Embraer airplane model, although the CFM's Dardo airplane is used for research, in order to have a more economical and practical solution.

Figure 6.1: CFM Dardo

To support the test campaign of the current configuration of the wing, a structural analysis is carried out using the Finite Element Method (FEM), through the use of FEMAP and NX Nastran. The main parts of wings are spars, stringers, ribs and skin, which in the FEM simulation are all modelled, in order to get accurate solutions for static, dynamic, buckling and aeroelastic analysis. It is worth noting that stringers are not used in the current configuration.

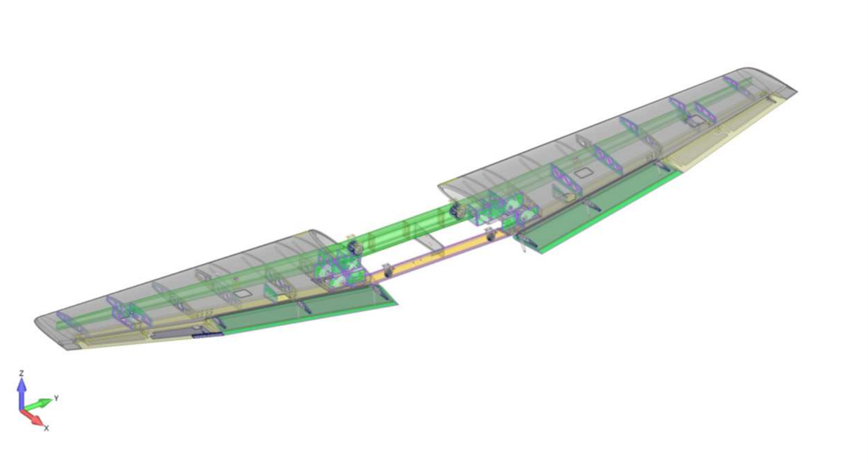

Figure 6.2: CAD model of the current DARDO's wing.

In the proposed study, the symmetry of the problem is exploited and only half of the wing is modeled in the FEM simulation. Figure 6.3 shows FEM mesh of the wing. All the components are modeled using plate linear elements of Nastran, i.e. four-node CQUAD4 and three-node CTRIA3 for laminates. Beam elements (CBEAM) are used for the L-shaped attachments between the main spar and the first rib. Rigid elements (RBE2 and RBE3) are also employed to link the external masses and loads to the wing structure. In total, the mesh accounts for around 27,000 elements (26,000 nodes). A brief description of the most important features of the FEM model is included in the following.

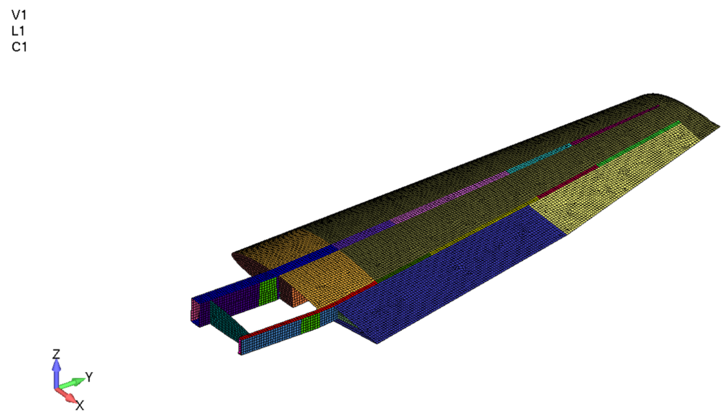

Figure 6.3: FEM model of the half wing.

6.2 Materials

The stacking sequence of each component of the wing is modelled using the PCOMP property, that allows the user to assign different materials with arbitrary thicknesses. In the following table are showed the different materials used in the wing model.

Material	E_1 [GPa]	E_2 [GPa]	G_{12}=G_{1z}=G_{2z} [GPa]	ν_{12}	$\rho \times 10^{-3}$ [kg/m^3]
Carbon fabric (FAB)	77.2	77.2	2.21	0.25	4.71
PVC foam (PVC)	1.0	1.0	0.28	0.25	0.075
Celeron (CEL)	7.0	7.0	2.0	0.25	1.4
Tape isotropic (ISO)	92.0	92.0	8.0	0.25	2.51
Tape unidir. (UNI)	109.0	8.0	2.21	0.25	4.71

Table 6.1: Materials used in the layups.

6.3 Boundary conditions

As stated above, due to the symmetry of the wing, only one half of the model is used for the analysis, so in order to impose the symmetry condition, displacement and rotations in x and z direction are blocked in nodes laying on the left-hand edge, as showed in Fig. 6.4. For the analysis two loading configurations are considered, ground test and in-flight test, with three different mass configurations. Every simulation is performed for a 225% of the limit load, which is obtained from the flight envelope and is equivalent to 3.8g.

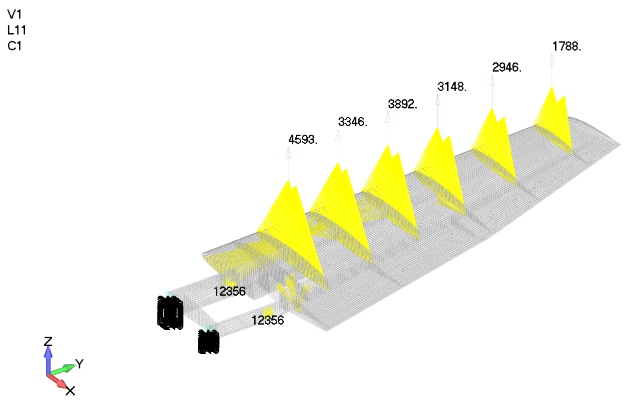

Figure 6.4

In ground test simulation the loading applied is that generated by the test rig, manufactured in order to accurately simulate the lifting forces on the wing. Those simulations allow us to validate the FEM model with experimental results. In order to model this type of loading, these forces are applied at virtual nodes linked to the ribs with a set of rigid connections (RBE2).
For the in-flight simulation, forces applied on the wing are obtained from a CFD analysis

and then modelled in the FEM simulation with a pressure load on the top skin.
In both of the simulations, three mass configurations are used:

- Empty weight: only the weight of the structure is used for the simulations;
- Landing weight in this configuration, weight of the landing gear is added. It results to be 15kg and is modelled as a non structural mass;
- Fuel weight: in this configuration, other than the landing gear weight, also the fuel is considered. It is modelled as a non structural mass of 40 kg.

6.4 Results

6.4.1 Static analysis

In Fig. 6.5 and Fig. 6.6 are showed the results for linear static analysis for ground test and in-flight condition, respectively. A further important point in static analysis, is the failure index which is showed in Fig. 6.7. It is showed the contour of the maximum failure index for ground test simulation, obtained with Tsai criteria. The maximum failure index results to be 0.753 and can be found in the spars at the root of the wing, as they are the most critical zones because of the maximum bending moment.

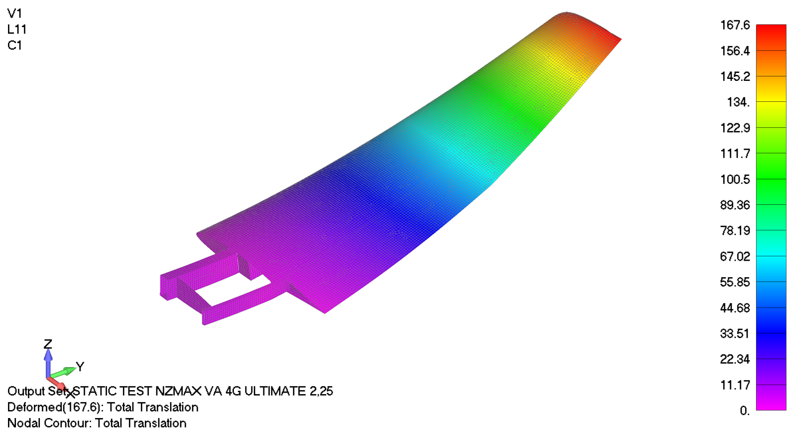

Figure 6.5: Ground test

6.4.2 Buckling analysis

For both configurations, ground test and in-flight analysis, also a linearized buckling analysis is performed. In Table 6.2 are showed the first five eigenvalues. For the different configuration, eigenvalues results to be similar and always greater than 1, meaning that the buckling will not happen for the 225% of the limit load but for a higher value.
Furthermore, as showed in Fig. 7.1, it can be noticed that the buckling will happen in panels in top skin, near the wing root.

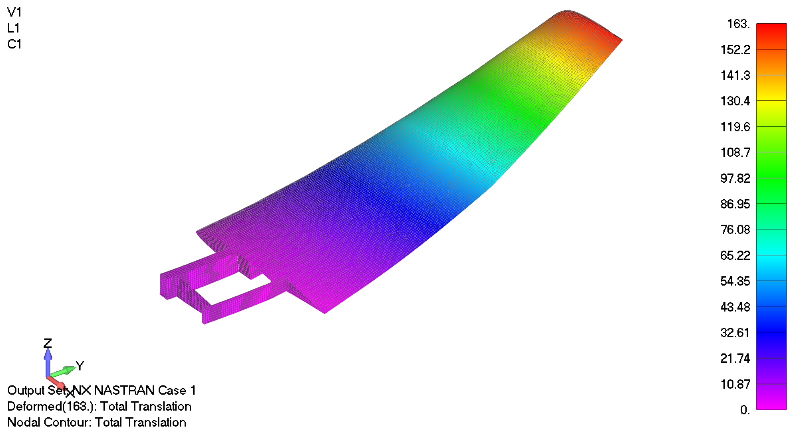

Figure 6.6: In-flight

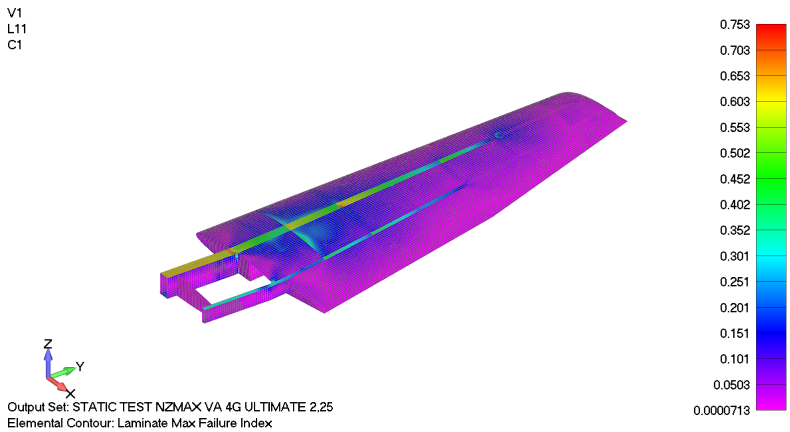

Figure 6.7

6.4.3 Free vibrations

Modal analysis is performed for every mass configurations. In Table 6.3 are showed the first ten natural frequencies for empty weight, landing weight and fuel weight. It can be observed that the mode that is less affected by the positioning of the extra mass is the first one (bending mode).

6.4.4 Flutter analysis

Flutter analysis is performed with the empty weight configuration. In Fig. 6.10 and Fig. 6.11 are showed the evolution of natural frequencies and damping with respect to $M = 0$ and sea level altitude. From those curves it is possible to obtain the flutter velocity and the flutter frequency, which are:

$$V_f = 249m/s, \qquad f_f = 48.8Hz.$$

Buckling mode	Ground test	In-flight
1	1.698	1.678
2	1.793	1.787
3	1.930	1.937
4	2.020	2.029
5	2.261	2.264

Table 6.2: First five buckling load factors for ground and in-flight loadings.

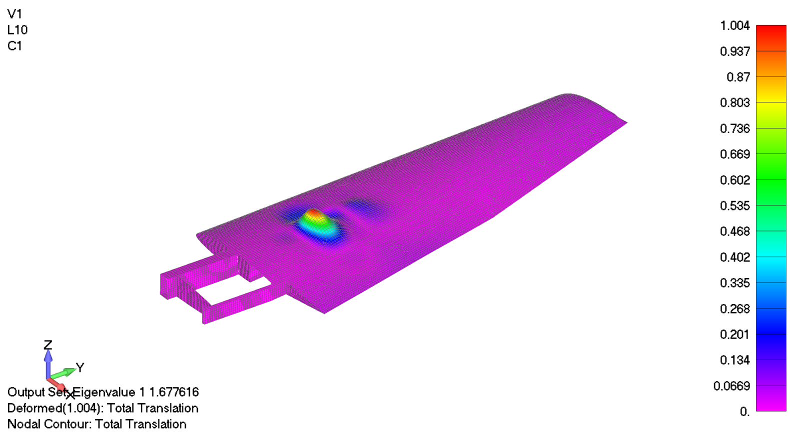

Figure 6.8

Flutter is triggered from the fourth mode, which is bending/torsion. In Fig. 6.12 is showed the shape of the fourth mode in flutter conditions.

	Empty weight	Including LG	Including LG + fuel
Mode 1	14.16	14.1	13.33
Mode 2	41.27	39.49	34.59
Mode 3	42.94	41.84	36.41
Mode 4	58.14	54.5	44.23
Mode 5	85.29	75.38	70.14
Mode 6	96.35	83.72	81.95
Mode 7	105.7	96.35	96.35
Mode 8	124.4	106.7	101.7
Mode 9	132.7	112.7	109.1
Mode 10	151.7	131.1	113.5

Table 6.3: First ten natural frequencies (Hz) of the wing for all three mass configurations.

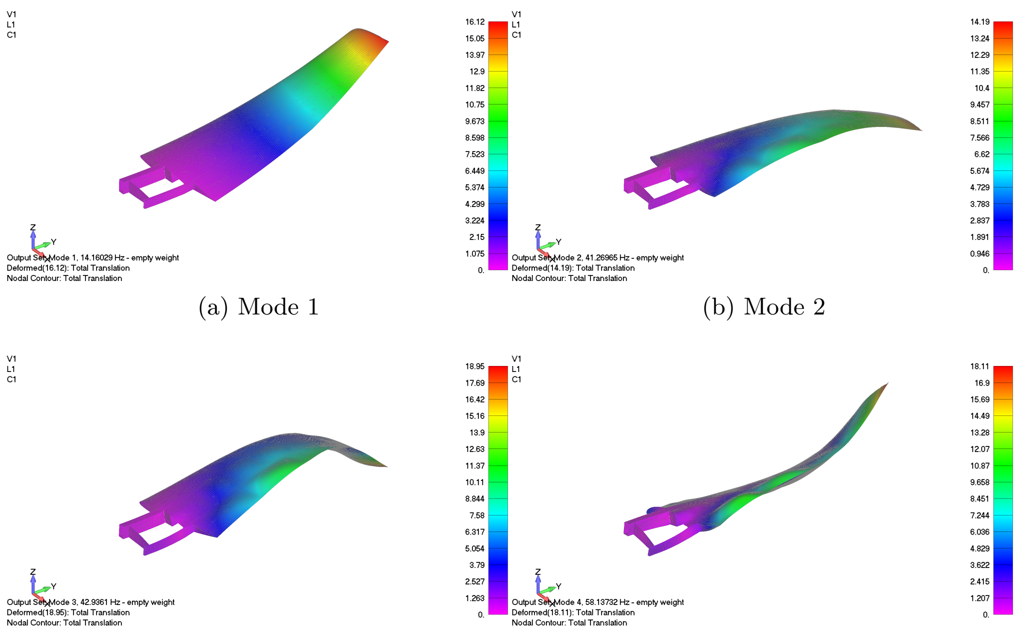

(a) Mode 1 (b) Mode 2

(c) Mode 3 (d) Mode 4

Figure 6.9: The first four modes of the empty wing.

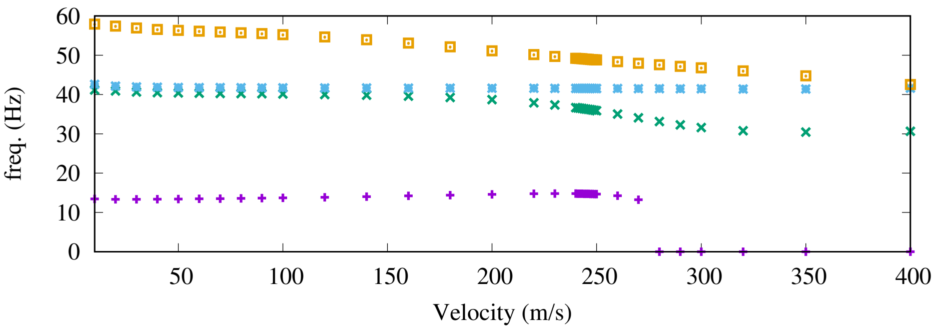

Figure 6.10: Variation of the modal values for increasing velocities.

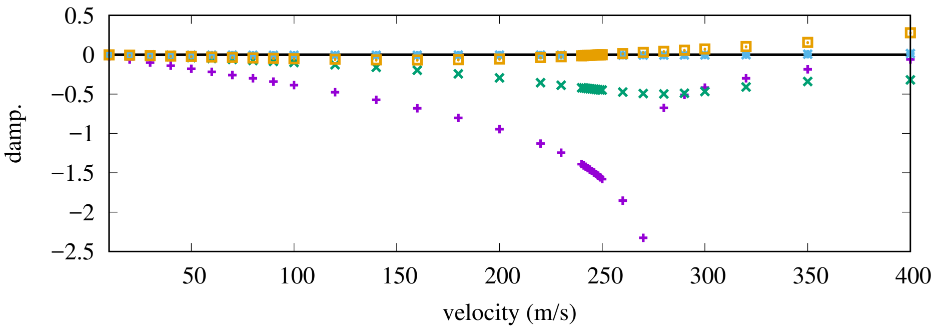

Figure 6.11: Variation of the damping values for increasing velocities.

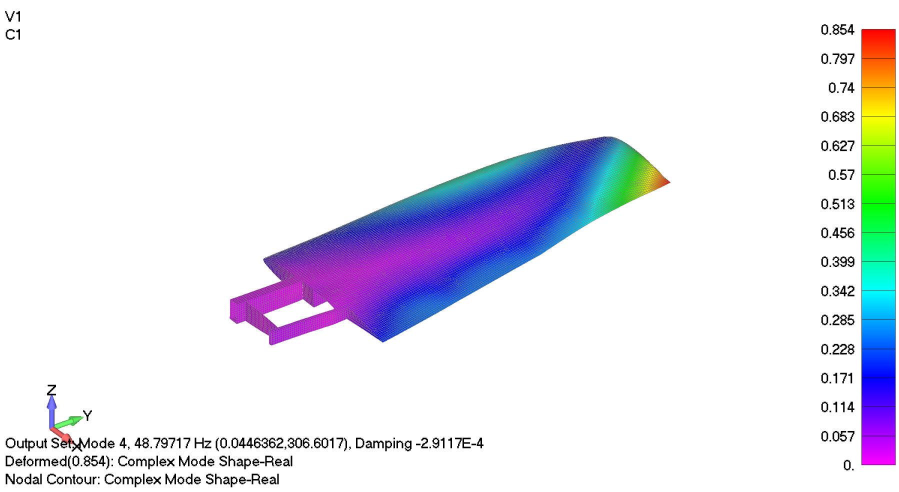

Figure 6.12: Shape of the 4^{th} mode at 249 m/s, $f = 48.8$ Hz.

Chapter 7

Dardo wing optimization

In the following chapter will be discussed the optimization analysis done for the CFM Dardo's wing. As stated in the previous chapters, one of the most important aspects for the optimization is to choose the formulation of the problem and, therefore, the number of design variables. We have seen that for small problems it is possible to directly manipulate the stacking sequence, using orientations and thicknesses as design variables, so that the dimension of the problem will be proportional to the number of plies of the laminate. The advantage of this approach would be to have immediate access to the optimized stacking sequence.
For our purpose using thicknesses and orientations as design variables could be non convenient, due to the large number of plies concerned. Hence, in the following optimization design lamination parameters will be used as design variables, in order to have a smaller problem.
Every analysis will be performed with Nastran, therefore Nastran default optimizer will be used, that is based on the gradient-based method that was introduced in Chapter 3.1.

7.1 Objective function

The objective of the following optimization will be to minimize the weight of the current Dardo's wing configuration, focusing on the value of the first buckling eigenvalue. As mentioned in Chapter 6 the buckling will happen for an higher value than the 225% of the limit load, more precisely at $\lambda_1 = 1.677$. The goal of the optimization design is to change the current stacking sequence in order to get the buckling at the 225% of the limit load, meaning that in this loading condition the first buckling eigenvalue should be $\lambda_1 = 1$.

7.2 Design variables

Every component will respond differently to each kind of objective and constraint that we can set, and, of course, some part can be more significant in certain analysis than other. In this particular case, since our main objective is to change the value of the first buckling eigenvalue, it has been chosen to optimize only the spar caps. In order to

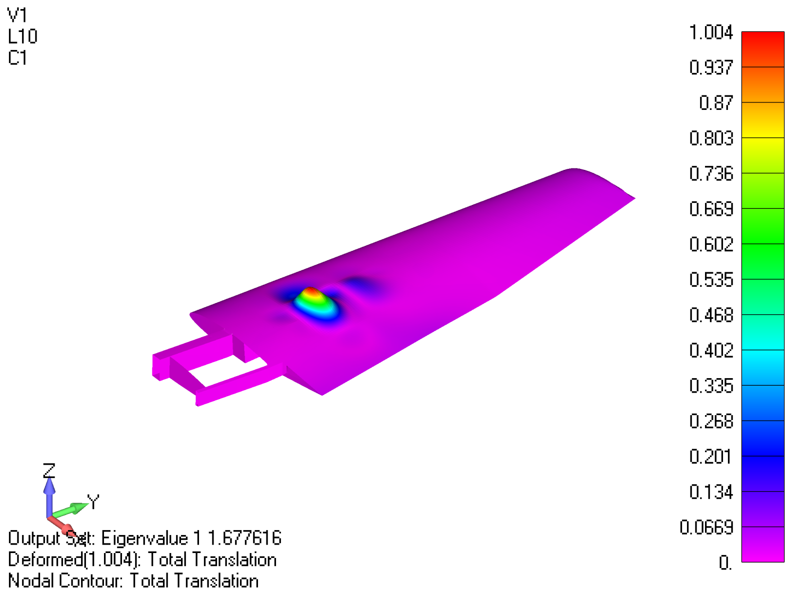

Figure 7.1: First buckling eigenvalue for the original wing stacking sequence.

obtain a meaningful solution, the spars are divided in different patches, whose lamination parameters will change during the optimization analysis. In Fig. 7.2 the patches are shown in different colors. The dimensions of the patches take into account the current stacking sequence, the loading on the wing and the blending and manifacturing constraints.

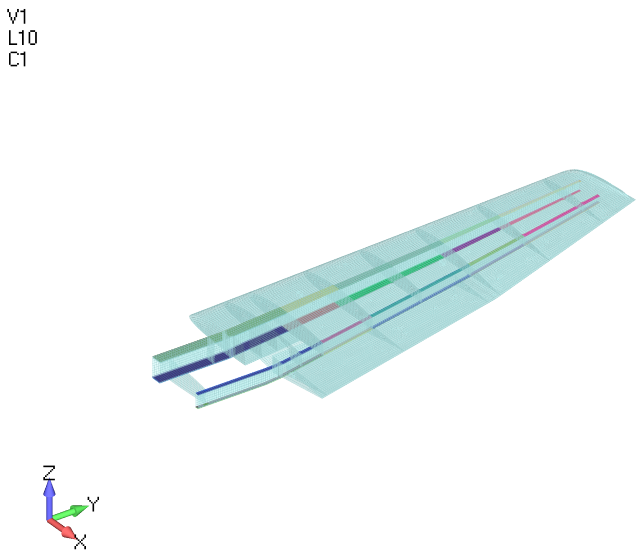

Figure 7.2: Patches for the spar optimization

7.3 Constraints

Since the optimization analysis is performed in the lamination parameters space, the first constraint to set is the feasibility constraint, represented by the following equations.

$$\begin{aligned}
&2(V_{1A})^2 - 1 \leq V_{2A} \leq 1 - (V_{3A})^2 \\
&2(1 + V_{2A})(V_{3A})^2 - 4V_{1A}V_{3A}V_{4A} + (V_{4A})^2 \leq [V_{2A} - 2(V_{1A})^2 + 1](1 - V_{2A}) \\
&2(V_{1D})^2 - 1 \leq V_{2D} \leq 1 - (V_{3D})^2 \\
&2(1 + V_{2D})(V_{3D})^2 - 4V_{1D}V_{3D}V_{4D} + (V_{4D})^2 \leq [V_{2D} - 2(V_{1D})^2 + 1](1 - V_{2D})
\end{aligned} \tag{7.1}$$

These equations shall ensure that the lamination parameters obtained will represent a feasible stacking sequence.
In order to take into account also the manifacturing constraint, will also be imposed the symmetry of the laminate and the standard angles.

- Symmetry constraint:

$$V_{1B} = V_{2B} = V_{3B} = V_{4B} = 0 \tag{7.2}$$

- Standard angles constraint:

$$V_{4A} = V_{4D} = 0 \tag{7.3}$$

7.4 Initial configuration

Forward spar caps

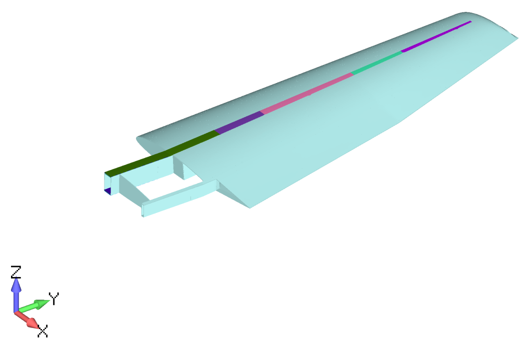

Figure 7.3: Forward spar caps patches

In Fig. 7.3 the patches for the forward spar caps are shown. In the initial configuration each patch is characterized with different stacking sequence, that will lead to different stiffness matrices and, hence, different lamination parameters. Each patch is made of carbon fabric and the material has been chosen to remain constant throughout the optimization process.

Patch	Stacking sequence	Thickness
1	$[-45/0_3/45/0_2/45/0_2/-45/0_3/45]$	$8.4mm$
2	$[-45/0_3/45/0_2/-45/0_2/45]$	$5.6mm$
3	$[-45/0_6/45]$	$4mm$
4	$[-45/0_3/45]$	$2.2mm$
5	$[-45/45]$	$0.4mm$

Rear spar caps

Similar to the forward spar caps, also the rear spar caps are divided in five different patches. In Fig. 7.4 is shown the configuration of the patches.

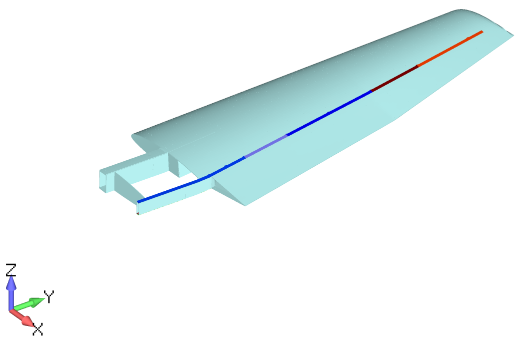

Figure 7.4: Rear spar caps patches

Patch	Stacking sequence	Thickness
1	$[-45/0_2/45/-45/0_2/45]$	$3.2mm$
2	$[-45/0/45/-45/0/45]$	$2mm$
3	$[-45/0/45]$	$1mm$
4	$[-45/45]$	$0.4mm$
5	$[-45/45]$	$0.4mm$

Weight and buckling eigenvalues

With the present stacking sequence the total weight of the spar caps is equal to $W_{spar,init} = 20.50kg$. The buckling eigenvalues obtained with this configuration are presented in the following table.

λ_1	1.677
λ_2	-1.680
λ_3	1.786
λ_4	-1.790
λ_5	1.937

7.5 Results and final configuration

Throughout the optimization process, lamination parameters of the second patch of the front spar are allowed to change, along with its thickness. Given the manufacturing constraint, only 6 lamination parameters will be used during the analysis, as stated in the previous paragraph. To sum up, the optimization problem for the spars can be expressed as the following.

- **Design objective**: weight minimization
- **Design variables**: 6 lamination parameters $(V_{1A}, V_{2A}, V_{3A}, V_{1D}, V_{2D}, V_{3D})$, 1 thickness
- **Constraints**: buckling eigenvalue ($\lambda_1 = 1$), feasibility and manufacturing constraints.

The comparison between the initial and final stiffness matrices is given below:

$$[A_i] = \begin{bmatrix} 568552 & 49049 & 0 \\ 49049 & 81518 & 0 \\ 0 & 0 & 35312 \end{bmatrix} \quad [A_f] = \begin{bmatrix} 223430 & 140270 & 0 \\ 0 & 223430 & 0 \\ 0 & 0 & 75340 \end{bmatrix}$$

$$[D_i] = \begin{bmatrix} 1428650 & 176564 & 0 \\ 176564 & 259770 & 0 \\ 0 & 0 & 121640 \end{bmatrix} \quad [D_f] = \begin{bmatrix} 223200 & 155170 & 0 \\ 0 & 223200 & 0 \\ 0 & 0 & 87620 \end{bmatrix}$$

Together with the lamination parameters and the stiffness matrices, also the thickness of the patch changed, specifically it decreased:

$$t_i = 5.6mm \quad t_f = 3.5mm$$

Thickness reduction is ensuring the desired weight reduction, while the variation of the stiffness matrices is changing the behaviour of the wing for the buckling. The new buckling eigenvalues are showed in the following table.

λ_1	1.002
λ_2	1.051
λ_3	1.305
λ_4	1.401
λ_5	1.662

At the end of the optimization the weight of the spars is reduced to $W_f = 20.04kg$. More specifically, focusing only on the second patch of the spar, the comparison between the initial and final weight is the following:

$$W_{init,patch2} = 1.18kg \quad W_{final,patch2} = 0.747kg$$

In Fig. 7.5 is shown the first buckling eigenvalue of the optimized wing.

As expected, the major changes happen in the terms of the D matrix, which is the one that directly affects the buckling behaviour, while the changes in the A matrix can be related to the feasibility and manufacturing constraints imposed.

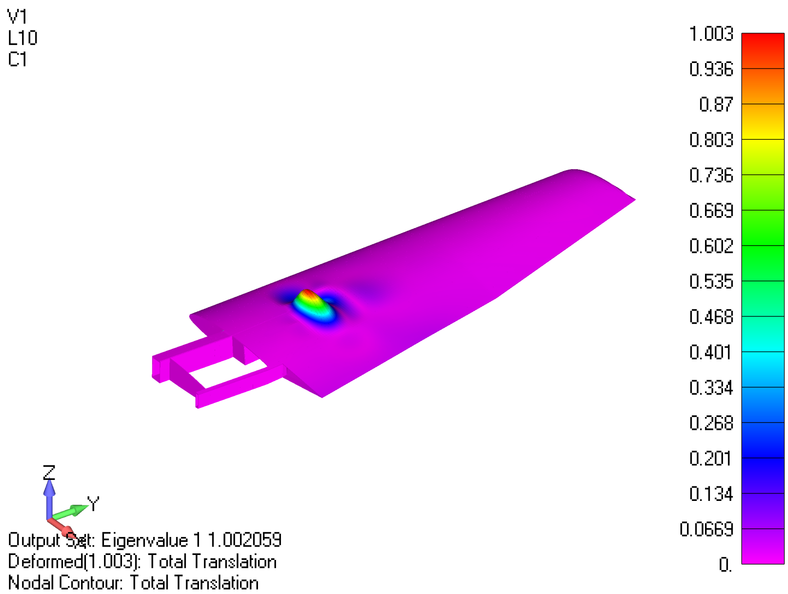
V1
L10
C1
1.003
0.936
0.87
0.803
0.736
0.669
0.602
0.535
0.468
0.401
0.334
0.268
0.201
0.134
0.0669
0.
Z
Y
Output Set: Eigenvalue 1 1.002059
Deformed(1.003): Total Translation
Nodal Contour: Total Translation

Figure 7.5

Chapter 8

Conclusions

The purpose of this thesis was to develop an efficient methodology to optimize the structure of a composite wing. This is a relevant subject in aeronautic industry, since one of the main goals of a project is to minimize the weight of the aircraft. Furthermore, weight reduction translates also into a reduction in consumption, providing an aircraft which is not only cost-effective, but also environmental friendly.
The optimization analysis is never trivial, since it's intrinsically a multidisciplinar problem and many issues must be take into account at the same time. First of all, when designing the code for the optimization analysis, it is important to choose properly which will be the variables that will govern the analysis. As seen in Chapter 2, composite materials can be described in different ways. Following the classical method, a laminate can be described through the orientations and thicknesses of each ply, which is the stacking sequence. Alternatively, the behaviour of a laminate can be also described through the stiffness matrices $[A], [B], [D]$, which can be, in turn, expressed as a linear combination of material invariants and lamination parameters. This implies that, in the optimization analysis, the design variables can be three different kind. In fact, it is possible to directly manipulate the stacking sequence (orientations and thicknesses), or the terms of the stiffness matrices, or the lamination parameters and the thickness. The choice of the design variables is a crucial point for the optimization analysis, since every relation (such as constraint equations) must be written in accordance to the variables. Furthermore, the choice of design variables can also affect the outcome of the analysis, both in terms of accuracy and time.
In Chapter 3 are described the principal algorithms nowadays used in design optimization, explaining the pros and cons. The choice of the algorithm is also influenced by the expression of the design variables. For instance, genetic algorithm are more indicated to the manipulation of the stacking sequence, since this kind of variables would be discrete. Gradient based algorithm can be used when working on stiffness matrices or lamination parameters, since these variables would be continuous.
In order to develop the optimization analysis for the Dardo's wing, it has been decided to use lamination parameters as design variables, in order to reduce the number of variables needed to describe the structure.
Another fundamental issue in optimization design concerns the understanding and the expression of the constraint to impose. As shown in Chapter 4, some constraint are directly related to the formulation chosen for design variables. In fact, in the present work, in

order to use lamination parameters as design variables, it has been necessary to set some feasibility constraint, that will ensure that the results obtained correspond to a real and feasible stacking sequence. There have been shown also the physical constraint, such as buckling and failure, and their formulation in the lamination parameter space.
In Chapter 6 was introduced the model of the current Dardo's wing, showing some details about the materials and boundary conditions, followed by the results of the most significant analysis.
In the final chapter, the knowledge acquired in the previous chapters, have been finally applied to the wing model, trying to obtain an optimized, lighter wing, imposing a buckling constraint. The optimization analysis has been performed on a section of the front spar cap. At the end of the analysis, the 36% of the weight was saved, leading to a lighter structure.

8.1 Future development

Even if the result obtained on the spar is remarkable, some extension to the developed optimization analysis can be envisaged. First of all, the expression of the manufacturing constraint and of the physical constraints can be improved, taking into account, for example, different physical constraints at the same time, which could be buckling analysis, flutter analysis and so on. Furthermore, in the present work the geometry of the wing remained constant throughout the optimization, changing only the lamination of the spars. In future works also the shape of the wing could be optimized, directly using mesh nodes coordinates as design variables.

Bibliography

[1] Z. Gurdal, R.T. Haftka, P. Hajela, *Design and optimization of laminated composite materials*, Wiley, 1999.

[2] Gustavo H. C. Silva, Alex Pereira do Prado, Pedro Higino Cabral, Roeland De Breuker, and Johannes K. S. Dillinger. *Tailoring of a Composite Regional Jet Wing Using the Slice and Swap Method*, Journal of Aircraft, 1–15

[3] S. Setoodeh, M. Abdalla, and Z. Gurdal. *Approximate Feasible Regions for Lamination Parameters*, 11th AIAA/ISSMO Multidisciplinary Analysis and Optimization Conference, Multidisciplinary Analysis Optimization Conferences, September 2006, Portsmouth, Virginia

[4] S. T. Ijsselmuiden, M. M. Abdalla, and Z. Gürdal. *Implementation of Strength-Based Failure Criteria in the Lamination Parameter Design Space* AIAA Journal, Vol. 46, No. 7 (2008), pp. 1826-1834

[5] G. Vanderplaats.*A robust Feasible Directions algorithm for design synthesis*, 24th Structures, Structural Dynamics and Materials Conference, Structures, Structural Dynamics, and Materials and Co-located Conferences

[6] G. Diaconu, Cezar and Sato, Masaki and Sekine, Hideki *Buckling characteristics and layup optimization of long laminated composite cylindrical shells subjected to combined loads using lamination parameters* Composite Structures, Vol. 58, No. 12 (2002), pp. 423-433

[7] Fukunaga H., Sekine H. *Stiffness design method of symmetric laminates using lamination parameters* AIAA Journal, Vol. 30, No. 11 (1992), pp. 2791-2793.

[8] E. Carrera, A. Pagani, E. Zappino, A.G. de Miguel *Static, dynamic and aeroelastic analyses of current design of CFM Dardo wing,* Technical report, Embraer, October 2018. A3.1